arXiv:1409.8628v1 [astro-ph.SR] 30 Sep 2014

To appear in Engle et al. 2014, ApJ, 794, 80

The Secret Lives of Cepheids: Evolutionary Changes and Pulsation-Induced Shock Heating in the Prototype Classical Cepheid δ Cep [1]

Scott G. Engle* and Edward F. Guinan

Department of Astrophysics and Planetary Science, Villanova University, Villanova, PA 19085 USA

scott.engle@villanova.edu

Graham M. Harper

School of Physics, Trinity College Dublin, College Green, Dublin 2 Ireland

Hilding R. Neilson

Department of Physics & Astronomy, East Tennessee State University, Box 70652, Johnson City, TN 37614 USA

and

Nancy Remage Evans

Smithsonian Astrophysical Observatory, MS 4, 60 Garden St., Cambridge, MA 02138 USA

ABSTRACT

Over the past decade, the *Secret Lives of Cepheids* (SLiC) program has been carried out at Villanova University to study aspects and behaviors of classical Cepheids that are still not well-understood. In this, the first of several planned papers on program Cepheids, we report the current results for δ Cep, the Cepheid prototype. Ongoing photometry has been obtained to search for changes in the pulsation period, light curve morphology and amplitude. Combining our photometry with the times of maximum light compilation by Berdnikov et al. (2000) returns a small period change of $dP/dt \approx -0.1006 \pm 0.0002$ sec yr^{-1}. There

*Centre for Astronomy, James Cook University, Townsville QLD. 4811, Australia

is also evidence for a gradual light amplitude increase of ∼0.011-mag (V-band) and ∼0.012-mag (B-band) per decade over the last ∼ 50 years. In addition, *HST-COS* UV spectrophotometry and *XMM-Newton* X-ray data were carried out to investigate the high-temperature plasmas present above the Cepheid photospheres. In total, from the five visits (eight exposures) with *XMM-Newton*, δ Cep is found to be a soft X-ray source ($L_{\rm X}$ [0.3–2 keV] $\approx 4.5-13\times10^{28}$ erg sec^{-1}) with peak flux at kT = 0.6–0.9 keV. The X-ray activity is found to vary, possibly in phase with the stellar pulsations. From 2010–2013, nine observations of δ Cep were carried out with *HST-COS*. The UV emissions are also variable, and well-phased with the stellar pulsations. Maximum UV line emissions occur near, or slightly before, maximum optical light, varying by as much as twenty times. This variability shows that pulsation-induced shock-heating plays a significant role in Cepheid atmospheres, possibly in addition to a quiescent, magnetic heating. The results of this study show Cepheid atmospheres to be rather complex and dynamic.

Subject headings: stars: activity — stars: atmospheres — stars: chromospheres — stars: coronae — (stars:) supergiants — (stars:) variables: Cepheids — stars: individual(δ Cep, β Dor, Polaris, SU Cas, ℓ Car, HD 213307, ξ^1 CMa) — ultraviolet: stars — X-rays: stars

1. Introduction

Classical Cepheids (Cepheids hereafter) are arguably the most important class of variable stars. From the *Leavitt* (*Period-Luminosity* = *P-L*) *Law*, these stars serve as crucial "standard candles" for determining the cosmic distance scale and measuring the Hubble Constant (H_0). Also, Cepheids play a fundamental role in the calibration of Type Ia supernovae, which indicate that the expansion of the Universe is accelerating, and also infer the existence of dark energy (Riess et al. 2011). In the near future, with the advent of missions such as *Gaia*, *JWST* and *WFIRST*, Cepheids will be employed to empirically measure the

[1]Based on observations made with the NASA/ESA *Hubble Space Telescope*, obtained at the Space Telescope Science Institute, which is operated by the Association of Universities for Research in Astronomy, Inc., under NASA contract NAS 5-26555. These observations are associated with programs #11726, #12302 and #13019. This work is also based on observations obtained with *XMM-Newton*, an ESA science mission with instruments and contributions directly funded by ESA Member States and the USA (NASA), associated with programs #055241, #060374 and #072354.

Hubble constant to $\sim 1\%$ (Freedman & Madore 2010). At this precision, and combining this directly measured H_0 with the results from *Planck* (Planck Collaboration et al. 2013) and *WMAP* (Komatsu et al. 2011) and those expected from *WFIRST*, the study of Cepheids will tightly constrain fundamental cosmological parameters.

Cepheids are also important astrophysical laboratories for probing the internal structure, stellar atmospheres and evolution of moderate mass ($\sim 4-15\ M_{\odot}$) stars (and Type II SN progenitors, for Cepheids above $\sim 8M_{\odot}$). For example, the study of Cepheids provides valuable information about convective core overshooting (Cassisi & Salaris 2011), mass loss (Neilson et al. 2012), rotation (Anderson et al. 2014) and helium core burning (Morel et al. 2010) for moderate mass, evolved stars. Studies of changes in their pulsation periods and amplitudes reveal evolutionary changes too subtle to detect directly, and understanding these various characteristics of Cepheids is crucial to their use as high-precision standard candles.

To this end, the *Secret Lives of Cepheids* (SLiC) program was initiated: a comprehensive study of Cepheid behavior, evolution, pulsations, atmospheres, heating dynamics, shocks and winds. The program started with the initially limited goal of photometrically monitoring the period and amplitude changes of Polaris (Davis et al. 2002; Neilson et al. 2012), and has since expanded to include 16 bright Cepheids, covering a wide range of pulsation properties (e.g. pulsation periods, amplitudes, modes of pulsation). The program now spans almost the entire electromagnetic spectrum, from recently acquired X-ray observations (*XMM-Newton* and *Chandra*), to FUV/UV spectra (*HST*, *IUE* and *FUSE*), to the ground-based photoelectric photometry we continue to gather, to high-resolution IR spectra (*SST*). Taken together, these data reveal Cepheids to be complex objects, with surprising levels of activity and behaviors. At optical wavelengths, we continue to monitor Cepheid light curves for possible signs of real-time stellar evolution, manifested by changes in light curve morphology, average brightness and times of maximum light. For example, in an increasing number of Cepheids, the pulsation period is known to change significantly, by as much as 200 sec yr^{-1} or more (Turner & Berdnikov 2004; Turner et al. 2007). Our photometry first indicated the recovery of Polaris' light amplitude (from its minimum value of $\sim$0.02-mag during the 1990s) in the early 2000s (Engle et al. 2004) and subsequent studies have confirmed our initial findings (Spreckley & Stevens 2008).

In addition to the evolutionary studies, we are investigating the atmospheric dynamics and heating of Cepheids using X-ray–UV data (the emphasis of this paper). Fokin et al. (1996); Gillet et al. (1999); Gillet & Fokin (2014) (and references therein) have shown variations in the atmospheric turbulence of Cepheids due to pulsation-driven shocks, and have discussed the effects (e.g. pulsation phase-dependent photospheric line broadening). During the 1980s and 90s, studies such as Schmidt & Parsons (1982, 1984a,b); Bohm-Vitense & Love

(1994), gathered numerous UV spectra of Cepheids with the *International Ultraviolet Explorer* (*IUE*), finding variable UV line emissions likely also due to shocks. Sasselov & Lester (1994) further calculated that this shock heating could produce X-ray emitting plasmas. These data, combined with the current study, all show Cepheid atmospheres to contain plasmas with temperatures of 10^3 – 10^7 K (Engle & Guinan 2012; Engle et al. 2009) that vary in phase with the pulsations of the Cepheids, indicating that the stellar pulsations are responsible for either the very presence, or at least the excitation, of the hot plasma emissions. The most likely mechanism, as discussed later, is pulsation-driven shocks propagating through the Cepheids' outer atmospheres. The detection and characterization of shocks in Cepheid atmospheres has become rather important in recent years as they may play a role in Cepheid mass loss (Marengo et al. 2010; Willson & Bowen 1986). The long exposures ($>$ 50 ksec) usually required for good X-ray characterizations have slowed progress in that wavelength range, but due to the excellent *HST Cosmic Origins Spectrograph* (*COS*) sensitivity, the UV–FUV situation is rather different. Typically, very good UV–FUV spectra are obtained in a single *HST* orbit.

2. δ Cep: The Prototype of Cepheids

δ Cep is an important calibrator for the *Period-Luminosity Law* because it has one of the most precisely determined distances ($d = 273 \pm 11$ pc from *HST Fine Guidance Sensor* (*FGS*) parallax determination) for a Cepheid (Benedict et al. 2007). This distance agrees well with the revised *Hipparcos* parallax distance of 265 ± 12-pc (van Leeuwen et al. 2007). Selected properties of δ Cep are given in Table 1, including two separate masses derived from either stellar pulsation theory or evolution models. The difference between the two values is a prime example of the *Cepheid mass discrepancy*, which has existed for decades (see Neilson et al. (2011)). Photometry of δ Cep dates back to its discovery light curve by Goodricke & Bayer (1786). It is also the second nearest Cepheid (only Polaris is nearer), and the member of a wide binary system with a hotter, A0V-type companion (HD 213307) at a projected distance of 40" away from the Cepheid (Prugniel et al. 2007). Further, δ Cep is a member of the Cep OB6 star cluster (de Zeeuw et al. 1999). Majaess et al. (2012) determined a cluster-derived distance of 277 ± 15 pc, which agrees very well with distances derived from parallax measures. Recently, a bow shock has also been found around the Cepheid, where the stellar wind is colliding with the surrounding interstellar medium, importantly constraining the mass loss rate to 10^{-7}–10^{-6} $M_\odot$ yr^{-1} (Marengo et al. 2010). This was confirmed by Matthews et al. (2012), using *Very Large Array* (*VLA*) H I 21 cm line observations to calculate a mass loss rate of $(\sim 1.0 \pm 0.8) \times 10^{-6}$ $M_\odot$ yr^{-1}.

Typical of many Cepheids, δ Cep displays the "saw tooth" light curve, with a quicker rise to maximum brightness, and a much slower decline to minimum brightness, as shown in Fig. 1. Because of its proximity (with respect to other Cepheids), δ Cep has been extensively studied at all wavelengths, including earlier UV studies (e.g. Schmidt & Parsons (1982, 1984a,b)) carried with the *International Ultraviolet Explorer* (*IUE*) satellite.

3. The Observations

3.1. Photometry

Photoelectric *UBVRI* photometry for this program was carried out with the *Four College Automatic Photoelectric Telescope* (*FCAPT* – Adelman et al. 2001) housed at *Fairborn Observatory*. The full data set was split to produce two well-covered light curves, centered at epochs 2008.9 and 2011.4. Fourier analyses of the resulting light curves yielded two times of maximum light, which were added to those found in the literature (Berdnikov et al. 2000). Our analysis of the complete timings dataset (Fig. 2) shows the period to be decreasing over time. From a quadratic fit to the O-C data, the rate of period change is calculated to be $\mathrm{dP/dt} = -0.1006 \pm 0.0002$ sec yr^{-1}, indicating that δ Cep is currently making its second crossing of the instability strip (Turner et al. 2007). According to theory, the star contracts and heats up during the second crossing, and its surface temperature rises. Thus, the average density of the star increases, resulting in a decrease in pulsation period, according to the *Period-Density Relation*

$$P \propto \frac{1}{\sqrt{\overline{\rho}}}$$

where P is the pulsation period and $\overline{\rho}$ is the average stellar density. Residuals of the quadratic O-C fit show no significant, additional (cyclic or otherwise) period variability.

B- and V-band light amplitudes of $\sim 1.31 \pm 0.013$- and 0.86 ± 0.010-mag, respectively, were also obtained from the individual *FCAPT* light curves, and compared to archival observations. From this comparison, the light amplitude of δ Cep appears to be increasing over time. If simple linear trends are assumed, the light amplitude of δ Cep has been increasing at a rate of ∼0.011-mag in the V-band and ∼0.012-mag in the B-band, per decade, over the last ~ 50 years (total changes of ~ 0.05 mag in V and ~ 0.06 mag in B – Fig. 3). It is interesting to note that many of the early observations of δ Cep, from the discovery of its variability in the late-1700s through to the early-1900s, display still smaller visual light amplitudes of $\sim 0.5 - 0.7$-mag (Hertzsprung 1919; Meyermann 1904). Known as a very capable and meticulous observer, Stebbins (1908) observed δ Cep with a polarizing photometer and reported a visual amplitude of 0.76-mag (though a fourier analysis of the data returned an

amplitude of 0.73-mag), based on observations made in 1906. These values would extend the amplitude trend observed in the past ~ 50 years (Fig. 3). However, these visual datasets require modern, careful calibrations before a conclusive determination of continued amplitude change can be achieved. In addition, the bottom panel of Fig. 3 shows that the average brightness of δ Cep has also increased over the same time span.

3.2. X-ray Observations

Constructing a theoretical model from spectroscopic observations, Sasselov & Lester (1994) concluded that Cepheids could produce X-ray activity via pulsation-induced shock-heating of their atmospheres. However, pointed *Einstein* and *Röntgen Satellite* (*ROSAT*) observations failed to detect any such activity, and indicated that Cepheids were not (at least significant) X-ray sources. Even with $log\ L_{\rm X} \approx 29$ erg s^{-1} (as determined by Sasselov & Lester), the problem with detecting X-rays from Cepheids is that these stars (except for Polaris at ~ 133 pc – van Leeuwen et al. (2007)) are far away, at $d > 250$ pc. Thus, they are expected to have relatively weak X-ray fluxes ($f_{\rm X} < 10^{-14}$ erg s^{-1} cm^{-2}). Though Polaris was detected, at the 3σ level, in a *ROSAT/High Resolution Imager* (*HRI*) archival image, the detection was not noticed until several years after the observation was carried out (see Evans et al. 2007). Confirmation of Polaris' X-ray activity and definitive detections of X-rays from other nearby Cepheids would not occur until the arrival of more powerful X-ray observatories such as *XMM-Newton* and *Chandra*.

We successfully obtained *Chandra* (PI: Evans) and *XMM-Newton* (PIs: Guinan & Engle) observations of five Cepheids – Polaris, δ Cep, β Dor, SU Cas and ℓ Car have been observed so far. The *Chandra* data reduction for Polaris is discussed in Evans et al. (2010). *XMM-Newton* data were reduced in the usual fashion, making use of the *Science Analysis System* (*SAS v13.0.0*) routines. Modeling of the *Chandra* and *XMM-Newton* data were then carried out using the *Sherpa* modeling and fitting package [distributed as part of the *Chandra Interactive Analysis of Observations* (*CIAO*) *v4.5* suite]. *MEKAL* models (Drake et al. 1996) were used for the final two-temperature (2-T) fitting and flux calculations.

3.3. X-ray Results

The nearest three Cepheids (and so far the only Cepheids detected) – Polaris, δ Cep & β Dor – have X-ray luminosities of $log\ L_{\rm X} \approx 28.6 - 29.2$ erg s^{-1}. Neither the short period Cepheid SU Cas ($P = 1.95$ d; $d = 395 \pm 30$ pc) nor the long period, luminous Cepheid ℓ Car

($P = 35.5$ d; $d = 498 \pm 55$ pc: Benedict et al. (2007)) were detected. Upper X-ray luminosity limits of $log\ L_{\rm X} \lesssim 29.6$ and 29.5 ergs s^{-1} were estimated for ℓ Car and SU Cas, respectively, based on exposure times, background count rates and stellar distances. Therefore, it is still possible that SU Cas and ℓ Car are X-ray sources with similar levels of activity to the Cepheids detected thus far, but are too distant to be detected above the background of the *XMM-Newton* exposures. However, the failure to detect two of our targets underscores a long-standing ambiguity present in the X-ray studies of Cepheids. Since Cepheids are young stars ($\sim 50 - 200$ Myr), any coeval main-sequence G-K-M companions (if present) would be coronal X-ray sources with X-ray luminosities similar to that of the Cepheids (see Guinan & Engle 2009, and references therein). Therefore, caution must be exercised as to whether unresolved companions are producing the X-ray activity. However, the *HST-COS* results (Engle & Guinan (2012), and this study) show plasmas with temperatures up to $\sim 10^5$ K that vary (in phase) with the Cepheids' pulsation periods. This indicates that plasmas approaching soft X-ray emitting temperatures do exist in Cepheid atmospheres.

As part of this study, five separate *XMM-Newton* visits were carried out for δ Cep. To provide better pulsation phase coverage, three of the visits were split during reduction into $\sim 30 - 50$ ksec sub-exposures, resulting in 8 individual exposures for analysis. Background-subtracted count rates were $\sim 0.002 - 0.006$ counts s^{-1} for all exposures. A neutral hydrogen ($N_{\rm H}$) column density value of 3.5×10^{20} ($log\ N_{\rm H} = 20.5$) cm^{-2} was adopted, based on distance relationships determined by Paresce (1984) and corroborated by target reddening (Ayres et al. 2005). The relevant two-temperature *MEKAL* model fitted parameters are given in Table 2. All X-ray energy distributions peak in the $kT \approx 0.6 - 0.9$ keV range ($\sim 7 - 10 \times 10^6$ K [MK]) and have measured flux values in the range of $\sim 4.5 - 13 \times 10^{-15}$ erg s^{-1} cm^{-2} (X-ray luminosities of $log\ L_{\rm X} \approx 28.6 - 29.1$ erg s^{-1}). The phased X-ray fluxes are shown in Fig. 4. The Cepheid's X-ray activity appears to reach a maximum near 0.5ϕ. This is different than what is found for the UV emission lines, which peak in the phase-range $0.9 - 1.0\phi$ (see Fig. 4). The nearby A0-type companion of δ Cep – HD 213307 – is also detected in the X-ray data, impying that this star may have a cooler, unresolved companion. For comparison, the X-ray flux of the companion star remains essentially constant in all exposures, while the X-ray flux of δ Cep increases by $2 - 3\times$ in the exposure near 0.5ϕ. Although our analysis has ruled out a possible flare or other transient events, this observation still represents a single (37 ksec) sub-exposure. A new (recently approved by *Chandra*) observation at similar phase will further investigate the high flux level. X-ray observations of β Dor ($P = 9.84$ days), the subject of a follow-up paper, show a similar flux increase at 0.5ϕ.

Possibly related to the X-ray variations reported here for δ Cep is the recent discovery by Oskinova et al. (2014) of small, pulsation-phased X-ray variations of the β Cep-type variable

star ξ^1 CMa. The periodic X-ray variations for ξ^1 CMa (HD 46328) have the same period as the fundamental stellar pulsation of this hot, magnetic B0.5 IV star. The X-ray fluxes peak near the optical maximum brightness that occurs near the minimum stellar radius and higest temperature. The relatively strong X-ray emissions observed for β Cep-type variables as well as other hot, massive stars arise from shock-heated winds (see Feldmeier et al. 1997). Oskinova et al. (2014) suggest that the periodic X-ray variations arise from small pulsation-induced changes in the wind structure, possibly coupled with changes in the magnetic field.

3.4. Ultraviolet Spectrophotometry

Prior to the installation of *HST-COS*, the most thorough UV studies of Cepheids were carried out in the 1980s–90s with the *International Ultraviolet Explorer* (*IUE*). Studies of particular note are the series of papers by Schmidt & Parsons (1982, 1984a,b) involving *IUE* data ($\sim 1200 - 3200$Å) for multiple Cepheids, including δ Cep, and Bohm-Vitense & Love (1994) which focused on the large available *IUE* dataset for the 35 day Cepheid ℓ Car. These studies found UV emission lines, including O I 1305Å, C IV 1550Å, and He II 1640Å, to vary with the Cepheid pulsation periods – evidence that the Cepheids (and not unseen companions) were responsible for the emissions, and pulsations may be the formation mechanism. The emissions are indicative of hot plasmas up to $100,000+$ K (also, He II can be partly formed via photoionization by coronal radiation – Pagano et al. (2000)).

One of the major aims of this study is to improve upon previous *IUE* results, since what appeared to be photospheric continuum flux introduced uncertainties in both emission line identifications and flux measures. *COS*, with finer spectral resolution, higher sensitivity and lower noise, can return superior spectra for which much more precise studies could be carried out. In addition, closely-spaced emission lines that were blended together in *IUE* spectra could be individually resolved in *COS* data and perhaps even less-prominent emission lines would be detected. Since the only reliable data in the $\sim 1200 - 1600$Å region available for Cepheids (at the beginning of this project) was low-resolution ($\sim 5 - 6$Å) *IUE-SWP*(R) spectra, it was quite frankly unknown exactly what the *COS* observations would show. The *HST-COS* spectra of δ Cep used in this study, and measured fluxes, are given in Table 3.

3.5. Ultraviolet Results

IUE was known to suffer from scattered optical light contamination (Basri et al. 1985), though it turned out to be much more of an issue than was anticipated. Fig. 5 shows a com-

parison of representative *IUE* and *COS* spectra for δ Cep. The improvement is dramatic. The much higher resolution was expected, but as the figure shows, a great deal of what could have been continuum flux from the photosphere turned out to be scattered light. This was the reason that *IUE* spectra of the program Cepheids could unambiguously show only the strongest emission lines (if any). In the case of Polaris, there was uncertainty as to whether any emission lines were present in the spectra; there was only a possible detection of the strong, but blended, oxygen/sulfur lines near $\sim$ 1300Å. The scattered light is not present in the *COS* spectra of Cepheids, however, which display a wealth of emission lines not detected in the archival *IUE* spectra. These lines define rich and complex Cepheid atmospheres and, as is well known, offer excellent atmospheric diagnostic potential (Linsky et al. (1995) and references therein), since different line species originate in plasmas of specific temperatures. Also, emission line strengths and ratios, as well as line broadening and radial velocities (RVs), when measured over the stars' pulsation cycles, offer important atmospheric diagnostics and can also help distinguish Cepheid supergiant atmospheric emissions from those of possible unresolved main sequence companions (if present). The flux values reported here are integrated fluxes for the emission lines with the continuum flux subtracted. To determine RVs for the emission lines, Gaussian fits were made

Although many important emission lines are present in the *COS* spectra, a few of importance were selected for the current study. These lines were selected because they represent a wide range of formation temperatures, and are relatively free from contamination via blending with nearby lines, offering a "pure" measurement of the emission line in question. The lines selected are:

- O I 1358Å – selected in favor of the well-known O I triplet at $\sim$ 1300Å because the triplet are fluorescent lines excited by H Lyman-β radiation (Koncewicz & Jordan 2007), suffer from blending with (primarily) nearby S I lines and heavy airglow contamination. Therefore, the flux of the O triplet is not necessarily indicative of plasmas at the O I peak equilibrium formation temperature of $1-2\times10^4$ K (Doyle et al. 1997).
- Si IV 1393/1403Å – a doublet with a peak formation temperature of $\sim 5-8\times10^4$ K (Linsky et al. 1995). This doublet represents an important link between the cooler, O I emitting plasmas and the hotter plasmas responsible for the N V and O V emission lines.
- N V 1239/1243Å – another doublet, but with a higher peak formation temperature of $\sim 1.5-2.5\times10^5$ K (Linsky et al. 1995). This doublet is very important because the lines occur at shorter wavelengths where photospheric continuum flux is essentially negligible. The N V doublet is the best measure of higher-temperature plasma variability in the UV spectra of the Cepheids.

- Additional Lines – Although not selected for a variability study due to its location on the red wing of the Lyman-α geocoronal-contaminated emission line, the O V 1218Å line is present in certain spectra and has a peak formation temperature of $\sim 2-4\times10^5$ K (Linsky et al. 1995). This places it among the hottest lines observable in the UV spectra of cool stars like the Cepheids, and its detection provides an important link to higher-temperature X-ray emissions. Additionally, measures have been made of the Si III 1206Å and 1298Å features, and the 1298/1206 flux ratio was used to carry out atmospheric density estimates.

Data accumulation and results in the satellite-based high-energy studies have been much slower than for the optical studies. However, δ Cep currently has the most complete phase coverage with *COS*. As an illustration of the results of the UV program thus far, the current *COS* light curves of δ Cep are given in Fig. 4. In looking at these plots, the most informative features are:

1. The phase at which line emissions begin to increase. The phase coverage of δ Cep has been illustrative in terms of the rise in emission flux. In comparing the emission line fluxes to the included photospheric RV plot for δ Cep, we see good correlation between the phase where UV line emissions begin to peak and a "pre-piston phase" as given by the RVs. During this pre-piston phase, the photosphere has almost reached its minimum radius, its recession is decelerating, and it is about to begin expanding again. Fokin et al. (1996) have shown that a shock should be propagating through the atmosphere of δ Cep at this phase ($\sim 0.8-0.85\phi$). The phasing of the flux increase is strong evidence in favor of a shock heating mechanism.

2. The abruptness of the increase in UV emissions from δ Cep is indicative of a sudden heating or excitation mechanism. Over a span of $\sim$ 10 hours (from $\sim 0.86-0.93\phi$), the O I 1358Å flux increases by $\sim 7\times$ (numbered points 4 – 7 in Fig. 4) and the Si IV flux increases by $\sim 10\times$. Such an abrupt, strong excitation also points to a shock-related mechanism. The decrease in flux is also rapid (though not as rapid as the increase), as one would expect for a sudden heating event such as a shock.

3. The presence of an apparent quiescent level of UV emissions during $0.6-0.8\phi$. This indicates a persistent atmospheric heating, possibly magnetic in origin, as is the case for numerous other classes of cool stars.

Another feature of note is the phase-difference between the peak flux of the most energetic (highest peak formation temperature) emission feature observed – N V $\sim$1240Å – and

the peak fluxes of the two cooler emission features. Unfortunately, for δ Cep, this aspect of the program requires a number of *very* narrowly phase-spaced observations that we simply do not have. Thus, a strict, quantitative conclusion cannot yet be drawn. However, the lower temperature plasma emission lines do appear to peak earlier than N V. In Fig. 4, spectrum 7 is clearly the most active spectrum in terms of O I 1358Å and Si IV 1393Å emissions. Qualitatively speaking, spectrum 7 looks to represent the peak phase of emissions for these two features. However, for N V emissions, spectrum 7 has nearly the same flux as spectrum 8. Since the overall shapes of the emission curves for these three features are so similar, it can be concluded that N V emissions are still rising in spectrum 7, where O I and Si IV emissions have essentially peaked. Thus, N V must have a peak emission slightly later ($\sim 0.02-0.03\phi$) in phase than O I and Si IV. As discussed by Bohm-Vitense & Love (1994), emissions from the hottest plasmas are expected to peak first in the case of shock-heating, followed by line emissions from cooling plasmas in the post-shock regions. However, its worth noting that the similarity of the rise times in UV line fluxes may result from the plasma exciting line emissions of various temperatures as it begins ionizing through to higher ionization states, and the process continues as the shock front moves through more neutral and singly ionized plasma. This is an interesting behavior, but one that will require more in-depth modeling and analysis before firm conclusions are drawn.

In addition to what is learned from emission line fluxes about the heating mechanism(s) at work in Cepheid atmospheres, the emission line profiles and RVs can provide valuable, complementary information. Fig. 6 gives the profiles of the O I 1358Å and Si IV 1393Å emission lines observed in several spectra of δ Cep. The most potentially informative characteristic is the asymmetry present in spectra 6–8, where the lines show a strong, additional blue-shifted emission component. This component is likely caused by an expanding shock emerging from the Cepheid photosphere. On the "near" side of the Cepheid atmosphere, the shock is approaching, producing the blue-shifted emission. In spectrum 8, the O I line still shows heavy asymmetry, but the Si IV line shows an extremely broad and even emission profile, indicative of a large velocity distribution but no additional blue-shifted feature. At this phase (0.04ϕ) we are likely observing Si IV emission from a very turbulent post-shock region, where the high turbulence is responsible for the velocity distribution, meaning that the shock has "passed by" the Si IV emitting region. The difference in O I and Si IV line profiles at this phase indicates that they are likely originating from different regions (heights) within the Cepheid atmosphere. The line profiles offer up further evidence in favor of shock-heating and compression being responsible for the enhanced emissions.

The RVs of the UV emission lines can give information on the workings of the δ Cep atmosphere, although we note there are *COS* wavelength calibration issues affecting their absolute accuracy (Aloisi et al. 2010). As such, the velocities can show a larger than normal

uncertainty, but the agreement in overall velocity trends between the three lines plotted gives confidence in the measures. In Fig. 7, the RVs (from top to bottom panels) of the O I, Si IV, N V emission lines and photosphere are plotted. As indicated in the figure, the emission line RVs have had the phase-specific photospheric RV removed. For the three emission line RV plots, the dashed gray horizontal line indicates zero velocity: when the line emitting region and the photosphere have identical velocities. Thus, line RVs above this line indicate that the line emitting region is compressing on to the photosphere, and line RVs below this line indicate the region is expanding away from the photosphere. In the bottom (photospheric RV) plot, the dashed gray horizontal line represents the average velocity of the star. For spectra where the Si IV and/or O I line showed asymmetry, two Gaussian profiles were fit to the line, and the RV of the broad atmospheric emission is plotted, as opposed to the blue-shifted emission component discussed in the previous paragraph. The agreement between the Si IV and O I velocity behaviors and that of the N V line, which maintained a symmetric single-Gaussian profile throughout the observed phases, gives confidence in the double-Gaussian approach.

Fig. 7 shows that, from $\sim 0.86 - 1.04\phi$ (spectra 4–8 in Fig. 4), the atmosphere of δ Cep is compressing on top of the photosphere. This compression begins just as the Cepheid photosphere is starting to expand again (the piston phase). This compression would result in further plasma excitation at these phases, contributing to the increased emission lines fluxes (Fig. 4) and line broadening (Fig. 6) that are observed.

Attempts have also been made to find suitable electron density-sensitive emission line ratios, to gain further physical insights into the Cepheid's atmosphere. A handful of well-studied ratios exist in the literature, making use of such emission lines as, e.g. C III (1909Å), Si III (1892Å) and O IV (∼1400Å). Unfortunately, either the spectra available for δ Cep do not cover the wavelengths of these emission lines (C III 1909Å or Si III 1892Å), or the lines are not strong enough to allow an unambiguous measurement (O IV ∼1400Å). Thus, none of these density measures could successfully be applied. Making use of the latest CHIANTI atomic database (http://www.chiantidatabase.org/) available at the time of writing (v7.1.3), investigations were carried out using a ratio of Si III line fluxes (1298/1206Å), as mentioned previously.

Measurements of almost all spectra for δ Cep give densities below the diagnostic range of the Si III 1298/1206Å ratio ($N_{\rm e} \lesssim 6 \times 10^9$ cm^{-3}). Spectrum 6 of δ Cep (as numbered in Figs. 4, 6), where the flux is steeply rising, gives a much higher density of $N_{\rm e} \approx 3.2 \times 10^{10}$ cm^{-3}. For reference, at similar plasma temperatures to those probed by the Si III ratio above, quiet regions of the Sun have measured densities of $\sim 5 \times 10^{10}$ cm^{-3} and active regions have densities of $\sim 1 \times 10^{10}$ cm^{-3} (Dupree et al. 1976), and other studies (Keenan et al. 1989,

e.g.) have also found solar densities to match that measured for spectrum 6 of δ Cep.

However, issues have been raised with using the Si III 1206Å line in density diagnostics. Dufton et al. (1983) calculated that, for the Sun, the 1206 line would be far too optically thick to give an accurate density. Although we believe that, in a supergiant such as δ Cep, the line would essentially be optically thin and suitable in that regard, there is also the temperature sensitivity to take into account when using a ground state transition, such as Si III 1206Å, with other subordinate features from higher levels. As such, we view the result as confirmation of increased atmospheric density during the phase of rising flux, but are still investigating the usefulness of the Si III ratio in returning a precise, numerical density measure.

All previously-mentioned features of the spectra support the conclusion that δ Cep's atmospheric plasmas are heated/excited via pulsation-driven compression and shock propagation.

4. Summary & Discussion

The prototype Cepheid δ Cep is undergoing some very interesting and complex behaviors. Optical photometry confirms that the pulsation period of the Cepheid is steadily decreasing over time at a rate of $\mathrm{dP/dt} = -0.1006 \pm 0.0002$ sec yr^{-1}. The decrease in the pulsation period indicates the star's radius is slowly decreasing as it contracts and evolves toward the blue (hotter) side of the H-R diagram. Also, standardized BV photoelectric photometry (from 1958–2012) provide evidence that the light amplitude and mean brightness are increasing. The observed changes in the light amplitude and average brightness of the star may also arise from slow evolutionary changes, indicating that we are witnessing stellar evolution in "real time."

Multiple X-ray observations and UV spectra have been taken of δ Cep with *XMM-Newton* and *HST-COS*. From these data, it is clear that δ Cep possesses an outer atmosphere of heated plasmas in the temperature range $T \approx 10^4 - 10^7$ K. Soft X-ray emissions are observed ($f_{\mathrm{X}} \approx 4 - 15 \times 10^{-15}$ erg s^{-1} cm^{-2}) with evidence of pulsation phase-dependent variability. This variability will need to be confirmed through an approved (*Chandra*), deep exposure taken at a similar phase. If the increased X-ray activity near 0.48ϕ is confirmed through additional data, the large difference between the phases of enhanced UV and X-ray emission will imply that perhaps competing (and at times, complementary) plasma-excitation mechanisms are at play in the Cepheid atmosphere.

The denser phasing of the *HST-COS* UV spectra have provided a clearer picture of the

$10^4 - 10^5$ K plasmas. Though a full astrophysical modeling of the data is underway and will have to be the topic of a future UV-dedicated paper, initial results from the spectra give a clear, general picture of the δ Cep atmosphere. UV emission line fluxes vary by a factor of $\sim 6 - 20\times$, depending on line species and plasma temperature (see Fig. 4), and the rise in emission line flux begins very near the phase of minimum stellar radius, just before the photosphere begins expanding again. This is the Cepheid "piston" phase, when a shock is expected to emerge from the photosphere and begin propagating through the atmosphere. Shortly after this phase, as the flux is increasing, the line profiles become asymmetric due to a blue-shifted emission feature (Fig. 6). This blue-shifted feature is caused by the additional excitation of plasma at the expanding shock front. During the phases of enhanced activity, the line profiles also noticeably broaden. This is a combination of the emergence of the blue-shifted feature, in addition to growing emissions from turbulent plasma in the post-shock regions and the overall compression of the atmosphere. This compression is seen in Fig. 7 during $\sim 0.86 - 1.04\phi$: while the photospheric recession slows, eventually turning to outward expansion, the atmosphere (as traced by emission line RVs) continues to recede, compressing around the photosphere. The phasing and strength of the flux increase, the line asymmetry and broadening of the line profiles and the photospheric vs. atmospheric RV behaviors all confirm that the atmospheric plasmas around δ Cep undergo regular excitation from the Cepheid's radial pulsations via atmospheric compression and shock propagation. The persistence of a quiescent atmosphere, outside of the shock-excited phase-range, indicates that a second heating mechanism, such as a stellar magnetic field, is also present in δ Cep.

5. Conclusions & Future Perspectives

The combined X-ray–UV–optical study of δ Cep, carried out under the SLiC program, shows the inherent complexity of this prototype Cepheid that underscores our (still incomplete) understanding of this important class of variable stars. Further, analyses of the long-term optical photometry provide strong evidence that relatively rapid evolutionary changes are taking place. This study demonstrates the high value of historical photometric data, in this case dating back to the time of Goodricke & Bayer (1786). Our study of time-series observations, from X-ray to optical wavelengths, are changing our perspective of these stars and have provided an initial step to understand not only Cepheid structures but also the details of their evolution and dynamic photospheres. We plan to continue high precision photometry to track the period change and also ascertain the observed small changes in the star's light amplitude and luminosity.

The *XMM-Newton* X-ray and *HST-COS* FUV spectrophotometry confirm the presence of variable, hot $\sim 10^4$ K-10^7 K plasmas in the outer atmosphere of this pulsating cool supergiant, most likely arising from pulsation-driven shocks. The similarity of the strengths of UV emissions (as well as X-ray luminosities) to some non-pulsating "hybrid" F–K giants and supergiants (Ayres 2011, and references therein) indicate that magnetic fields could also play a role in the origin of these high-energy emission lines. Although the presence of phase-dependent FUV line emissions was expected from prior *IUE* studies of Cepheids, the X-ray emissions (especially the possible $L_{\rm X}$ variability) is very surprising and is being followed-up.

The pulsation shock heating of the atmosphere of δ Cep (and, by extension, of other Cepheids) has yet undetermined effects on the energetics, heating, structure and dynamics of Cepheid atmospheres that could effect the *P-L Law*. As discussed previously, if Cepheids are to be used to significantly improve the cosmic distance scale and precisely determine the Hubble Constant (H_0) to an uncertainty of $\sim$1%, it will be necessary to have a clearer understanding of the effects of the pulsation-induced shocks on Cepheid atmospheres. The deposition of shock-induced energies in the outer atmosphere could affect the luminosity and pulsations of the stars. As additional targets are analyzed, the SLiC program will address these problems with a larger sample of stars. In forthcoming papers we will present the results for additional representative Cepheids that include Polaris, β Dor, and ℓ Car. Finally, we will continue to carry out ground-based photometry and to request additional space-based observations to help unlock the secret lives of these stars.

The authors wish to thank the tireless efforts of Lou Boyd, *Fairborn Observatory* Director, in maintaining the *FCAPT*.

The authors also wish to thank the financial support of NSF grant AST05-07542, and NASA grants HST-GO11726, HST-GO12302, HST-GO13019 and XMM-Newton: NASA NNX14AF12G.

Support for *HST* programs 11726, 12302 and 13019 was provided by NASA through grants from the Space Telescope Science Institute, which is operated by the Association of Universities for Research in Astronomy, Inc., under NASA contract NAS 5-26555.

Facilities: XMM-Newton, Chandra, HST (COS).

Table 1. Relevant Stellar Properties of δ Cep.Table 1

Parameter	Value
Spectral Type	F5Ib – G1Ib[1]
$T_{\rm eff}$ (K)	$5500 - 6600$[1]
Mass (pulsational) ($M_\odot$)	4.5 ± 0.3[2]
Mass (evolutionary) ($M_\odot$)	5.7 ± 0.5[2]
Mean Luminosity ($L_\odot$)	~ 2000[3]
Mean Radius ($R_\odot$)	44.5[3]
Distance (pc)	273 ± 11[4]
$\langle V \rangle$-mag	3.89 ± 0.010*
V-band Amplitude	0.86 ± 0.010*
Ephemeris (this study): $2455479.905 + 5.366208(14) \times E$	
Ephemeris for O-C diagram (Berdnikov et al. 2000): $2412028.956 + 5.3663671 \times E$	

[1]Andrievsky et al. (2005)

[2]Caputo et al. (2005)

[3]Matthews et al. (2012)

[4]Benedict et al. (2007)

*this study

Table 2. *XMM-Newton* Observations of δ CepTable 2

Observation ID #	Start Time (UT)	End Time (UT)	Start Phase	End Phase	$N_{\rm H}$ ($\rm cm^{-2}$)	Temp. (keV)	Temp. Ratio	$f_{\rm X}(0.3-2.5keV)$ ($10^{-15}ergs^{-1}cm^{-2}$)	$f_{\rm X}$ error ($10^{-15}ergs^{-1}cm^{-2}$)	$L_{\rm X}$ ($ergs^{-1}$)	$log\ L_{\rm X}$
0603740901	2006/01/19 18:04	2006/01/20 12:37	0.054	0.12		0.254	1.00	6.070	3.000	5.382E+28	28.73
	2455217.253	2455218.026				0.704	0.63				
0603741001_I	2006/01/21 18:05	2006/01/22 14:17	0.43	0.51		0.618	0.29	15.040	2.000	1.334E+29	29.13
	2455219.254	2455220.095				2.115	1.00				
0603741001_II			0.51	0.58		0.353	0.48	8.172	2.000	7.246E+28	28.86
						1.345	1.00				
0552410401	2004/06/4 14:26	2004/06/4 21:53	0.332	0.39		0.995	1.00	5.130	1.500	4.549E+28	28.66
	2454623.101	2454623.412			3.5E+20	0.401	0.64				
0723540301_I	2013/06/28 6:34	2013/06/29 13:49	0.84	0.96		0.321	0.97	4.340	1.000	3.848E+28	28.59
	2456471.774	2456473.076				1.328	1.00				
0723540301_II			0.96	0.08		0.408	1.00	4.350	2.200	3.857E+28	28.59
						1.378	0.65				
0723540401_I	2013/07/2 6:17	2013/07/3 7:51	0.58	0.68		0.613	1.00	3.710	0.700	3.290E+28	28.52
	2456475.762	2456476.827				0.741	0.01				
0723540401_II			0.68	0.78		0.361	1.00	5.944	1.500	5.270E+28	28.72
						0.956	0.42				

Note. — Temp. Ratio refers to the relative contributions of each plasma temperature to the overall 2-temperature fit. They are normalized such that the more prominent temperature has a contribution factor of 1.
Observation #'s ending with _I and _II represent the first and second halves of a split observation.

Table 3. HST-COS Observations of δ CepTable 3

Observation ID #	Start Time (UT)	End Time (UT)	Phase	Exp. Time (sec)	COS Grating	Central λ (Å)	N v 1240Å Flux (Sum)	N v Flux Error	O i 1358Å Flux	O i Flux Error	Si iv 1400Å Flux (Sum)	Si iv Flux Error
LBK809010	2010/10/19 00:12	2010/10/19 00:30	0.610	924.992	G130M	1291	1.379E-15	3.203E-16	1.085E-15	1.885E-16	1.765E-15	4.519E-16
LBK809020	2010/10/19 01:30	2010/10/19 01:48		923.968	G160M	1589						
LBK817010	2010/12/12 06:12	2010/12/12 06:29	0.715	924.992	G130M	1291	1.687E-15	3.675E-16	1.163E-15	2.658E-16	2.239E-15	4.311E-16
LBK817020	2010/12/12 06:34	2010/12/12 06:52		923.904	G160M	1589						
LBK818010	2010/10/30 16:24	2010/10/30 16:41	0.782	924.96	G130M	1291	1.482E-15	3.015E-16	1.198E-15	2.405E-16	1.979E-15	4.326E-16
LBK818020	2010/10/30 16:54	2010/10/30 17:11		923.968	G160M	1589						
LBK819010	2010/10/31 04:04	2010/10/31 04:22	0.872	925.024	G130M	1291	1.680E-15	2.978E-16	3.068E-15	3.159E-16	3.674E-15	6.304E-16
LBK819020	2010/10/31 04:26	2010/10/31 04:44		924.032	G160M	1589						
LBK820010	2010/12/13 23:42	2010/12/14 00:00	0.041	925.024	G130M	1291	8.000E-15	4.657E-16	4.461E-15	4.089E-16	1.831E-14	1.142E-15
LBK820020	2010/12/14 00:04	2010/12/14 01:13		924.032	G160M	1589						
LBK821010	2010/10/22 01:41	2010/10/22 01:59	0.180	925.024	G130M	1291	4.063E-15	3.777E-16	1.681E-15	2.540E-16	4.906E-15	5.904E-16
LBK820020	2010/10/22 02:56	2010/10/22 03:14		924.032	G160M	1589						
LBK822010	2010/10/31 02:28	2010/10/31 02:46	0.860	925.024	G130M	1291	1.848E-15	3.016E-16	1.703E-15	2.452E-16	3.063E-15	5.278E-16
LBK822020	2010/10/31 02:50	2010/10/31 03:08		924.032	G160M	1589						
LBK823010	2010/10/29 22:59	2010/10/29 23:28	0.647	924.928	G130M	1291	1.492E-15	3.303E-16	1.198E-15	2.363E-16	2.088E-15	4.451E-16
LBK823020	2010/10/29 23:32	2010/10/29 23:50		923.936	G160M	1589						
LBK815010	2011/06/13 16:50	2011/06/13 17:12	0.901	1152.032	G130M	1291	2.845E-15	3.200E-16	6.053E-15	3.722E-16	1.197E-14	6.869E-16

Table 3—Continued

Observation ID #	Start Time (UT)	End Time (UT)	Phase	Exp. Time (sec)	COS Grating	Central λ (Å)	N v 1240Å Flux (Sum)	N v Flux Error	O i 1358Å Flux	O i Flux Error	Si iv 1400Å Flux (Sum)	Si iv Flux Error
LBK815020	2011/06/13 17:17	2011/06/13 17:37		1024.032	G160M	1589						
LC2307010	2013/01/18 18:29	2013/01/18 18:49	0.933	767.008	G130M	1291	7.496E-15	6.732E-16	1.099E-14	7.579E-16	3.460E-14	1.696E-15
LC2307020	2013/01/18 18:52	2013/01/18 20:12		763.072	G160M	1589						

Note. — All fluxes and errors given in erg s^{-1} cm^{-2}

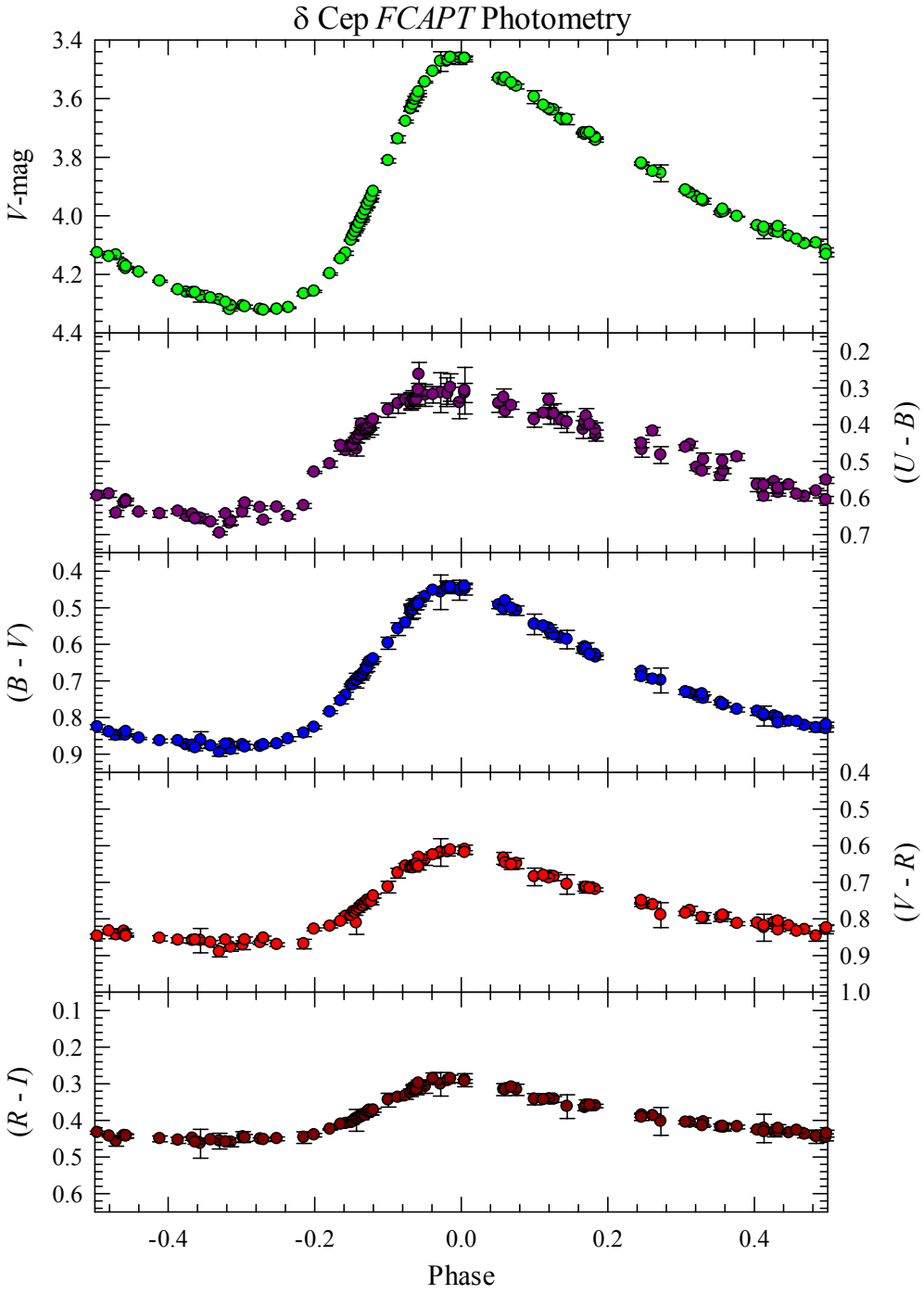

Fig. 1.— *UBVRI* photometry of δ Cep obtained with the *FCAPT*. The ephemeris used for phasing is that given in Table 1.

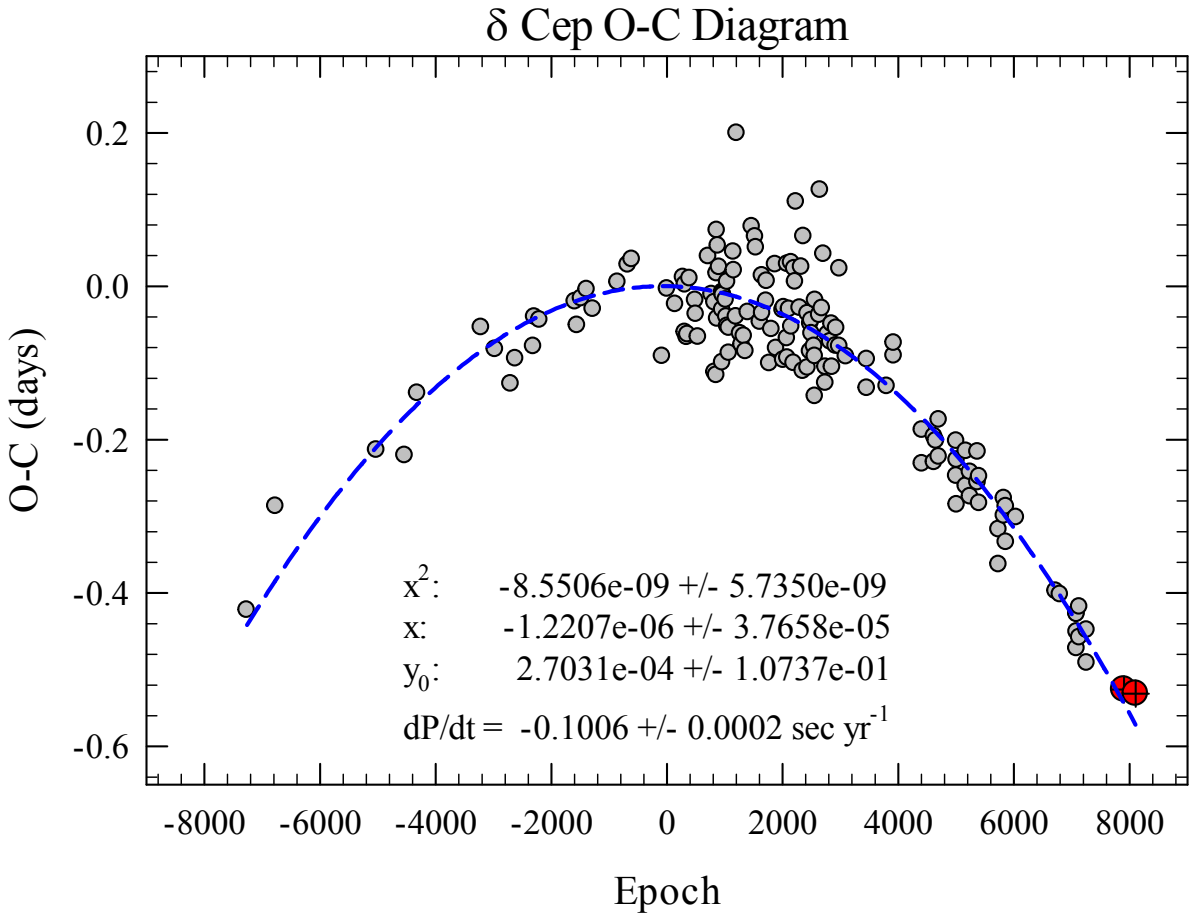

Fig. 2.— The O-C diagram for δ Cep. The region of larger scatter from epochs $\sim 0 - 3000$ (timespan $\sim 1900 - 1940$) represents the period of time when unaided (naked-eye) visual observations of bright variables such as δ Cep were being carried out by numerous observers. The combined effects of varying observer experience, methodologies and even observing sites gives rise to the increased scatter (see Berdnikov et al. (2000) for details of the archival timings dataset.) The quadratic fit parameters, which return a period change of $dP/dt = -0.1006$ sec yr^{-1}, are given in the plot, and the steadily decreasing period trend can be seen.

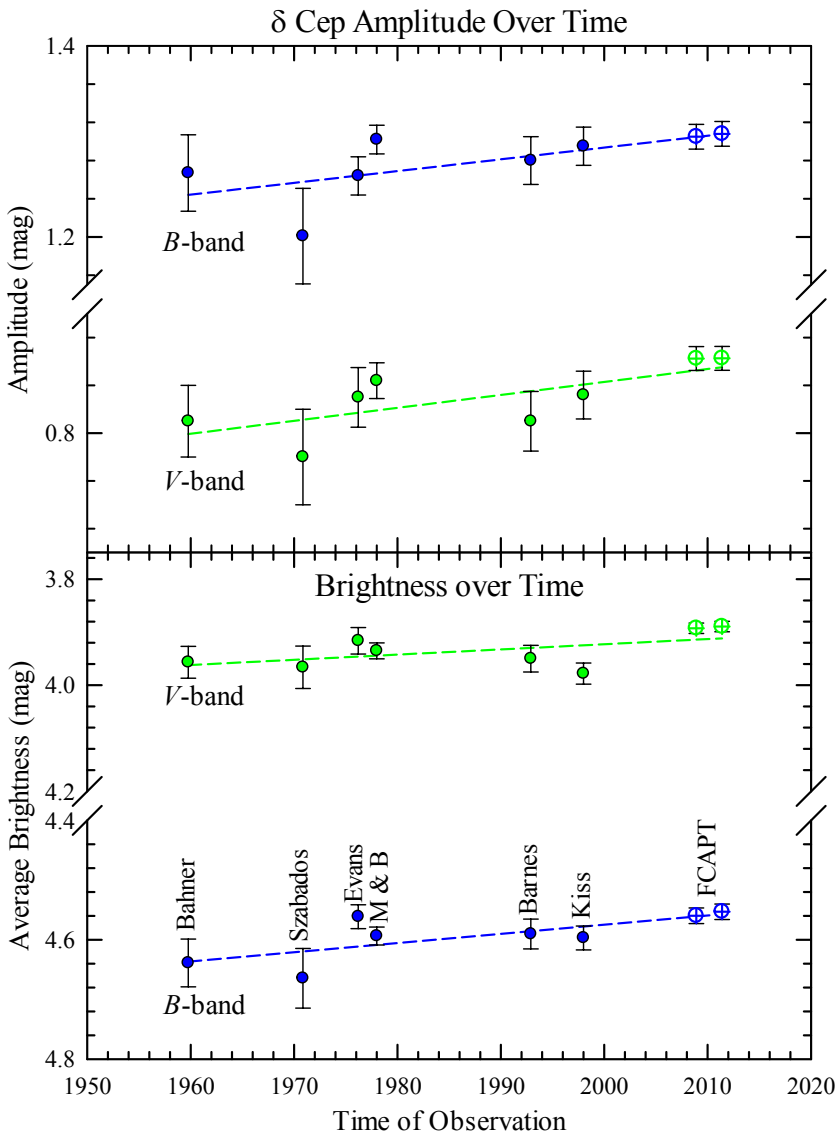

Fig. 3.— The top panel plots light amplitudes of δ Cep over time, and the bottom panel plots the average brightness of the Cepheid. Only studies where standard Johnson B- and V-filter data were obtained have been included in the plots. Fitting linear trends to the data show that the light amplitude of δ Cep has increased at an average rates of $\sim$0.011 mag (V) and $\sim$0.012 mag (B) per decade. In the same time span, the average brightness of δ Cep has increased by $\sim$0.01 mag (V) and $\sim$0.02 mag (B) per decade. Archival photometry was obtained from: Kiss (1998); Barnes et al. (1997); Moffett & Barnes (1980); Evans (1976); Szabados (1980); Bahner et al. (1962). The photometry carried out in this study made use of the same comparison stars as Barnes et al., Moffett & Barnes, and Evans.

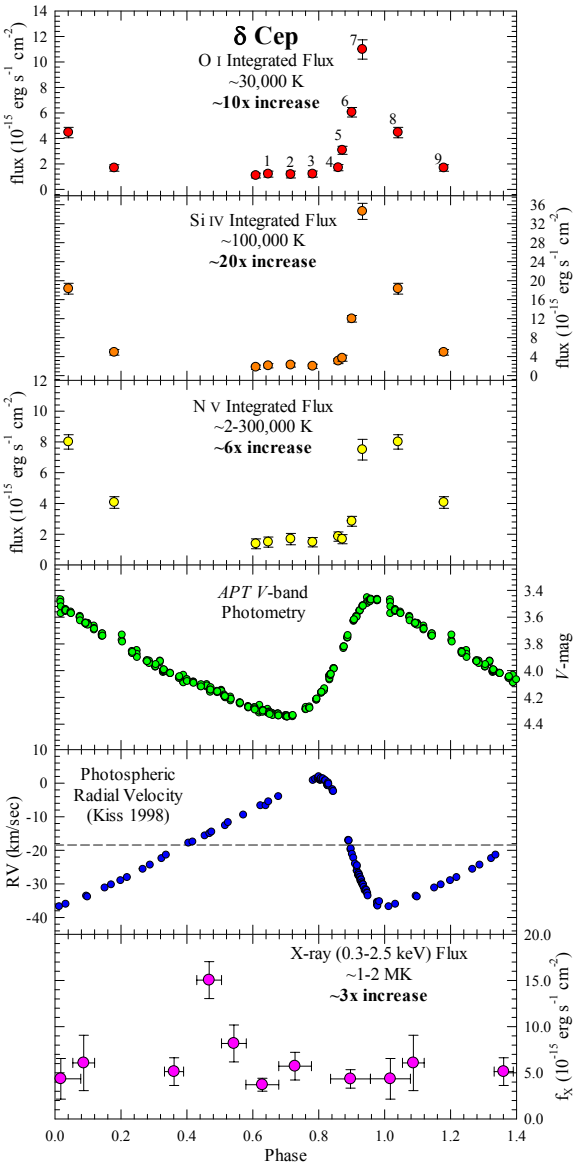

Fig. 4.— The top three panels show integrated fluxes measured from *COS* spectra of δ Cep. The fourth panel shows the V-band lightcurve obtained by us, the fifth panel shows the photospheric RVs from Kiss (1998), and the sixth panel shows the X-ray fluxes derived from two-temperature fits to the *XMM-Newton* data. Several flux-points in the top panel are also numbered for comparison to the line profiles plotted in Fig. 6.

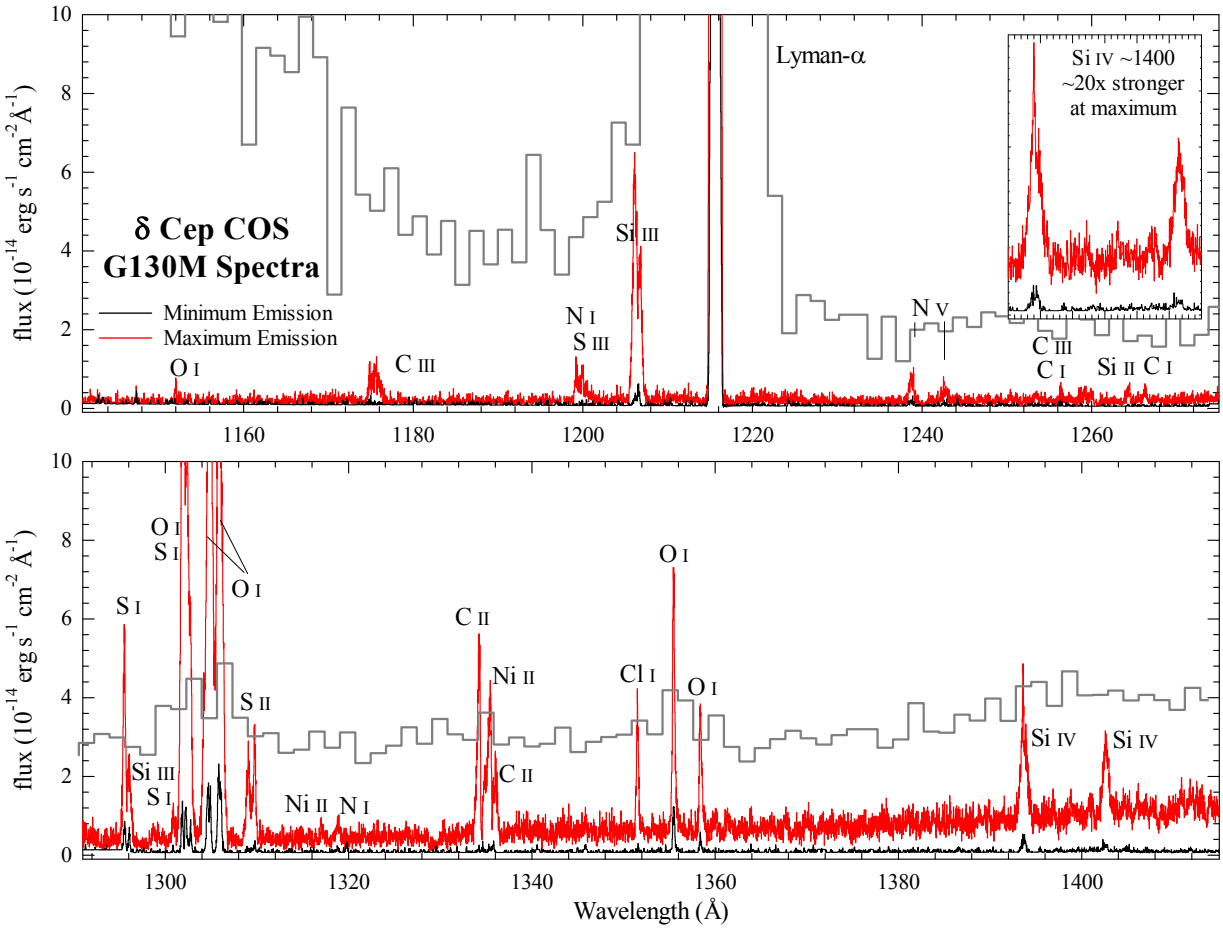

Fig. 5.— A comparison of *IUE* (gray, low-res histogram) and *COS* (red and black for max/min activity levels) spectra for δ Cep. Emission lines that are very well-characterized in the *COS* spectra barely reveal themselves (or are absent altogether) in the scattered-light-contaminated *IUE* data.

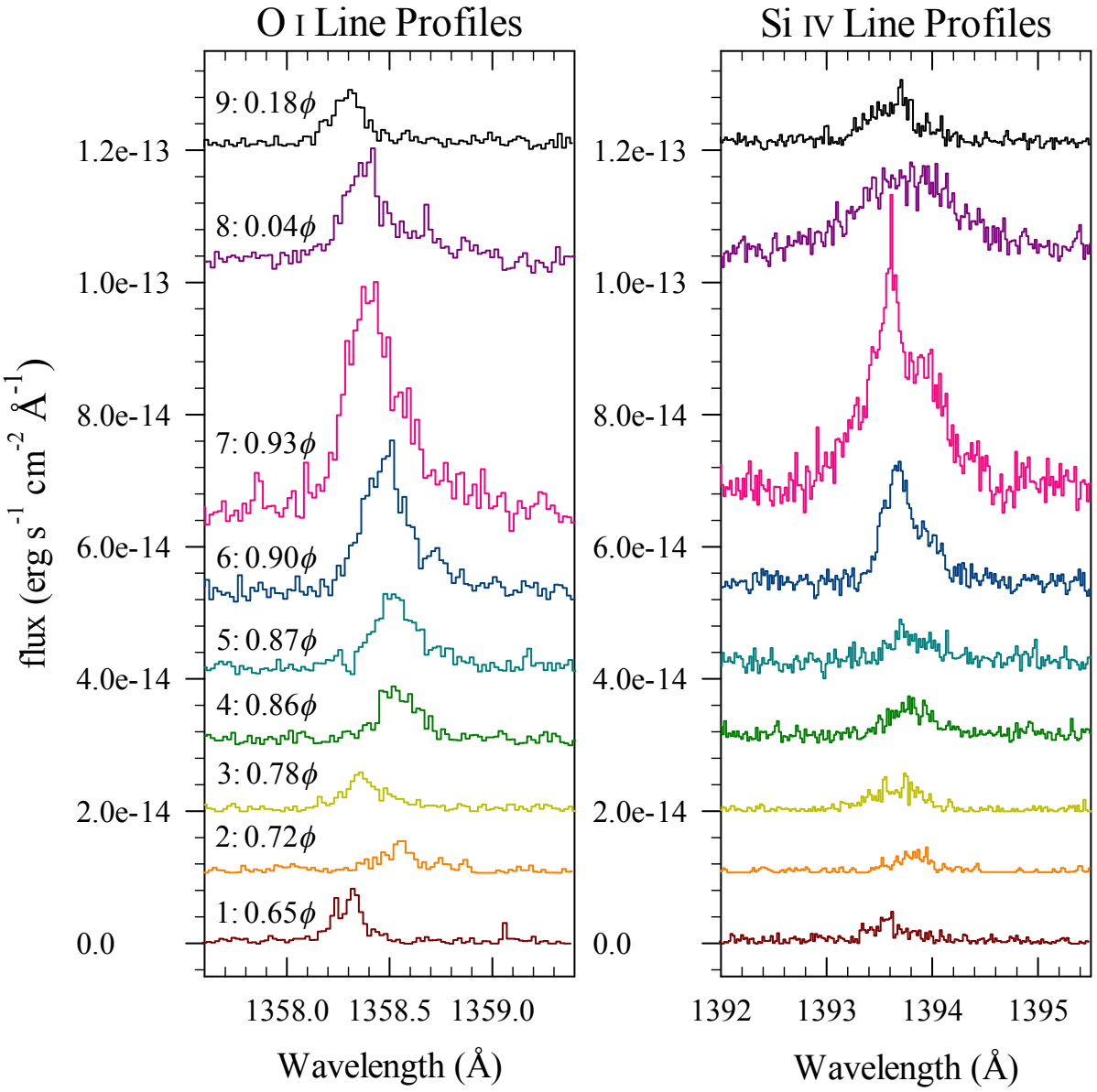

Fig. 6.— The O I 1358Å and Si IV 1393Å line profiles are plotted for δ Cep. The spectra are numbered, according to Fig. 4. The difference in emission strengths can be seen, along with the asymmetries present at several phases, caused by the emergence of an additional blueward emission feature during phases where a shock is propagating through the atmosphere.

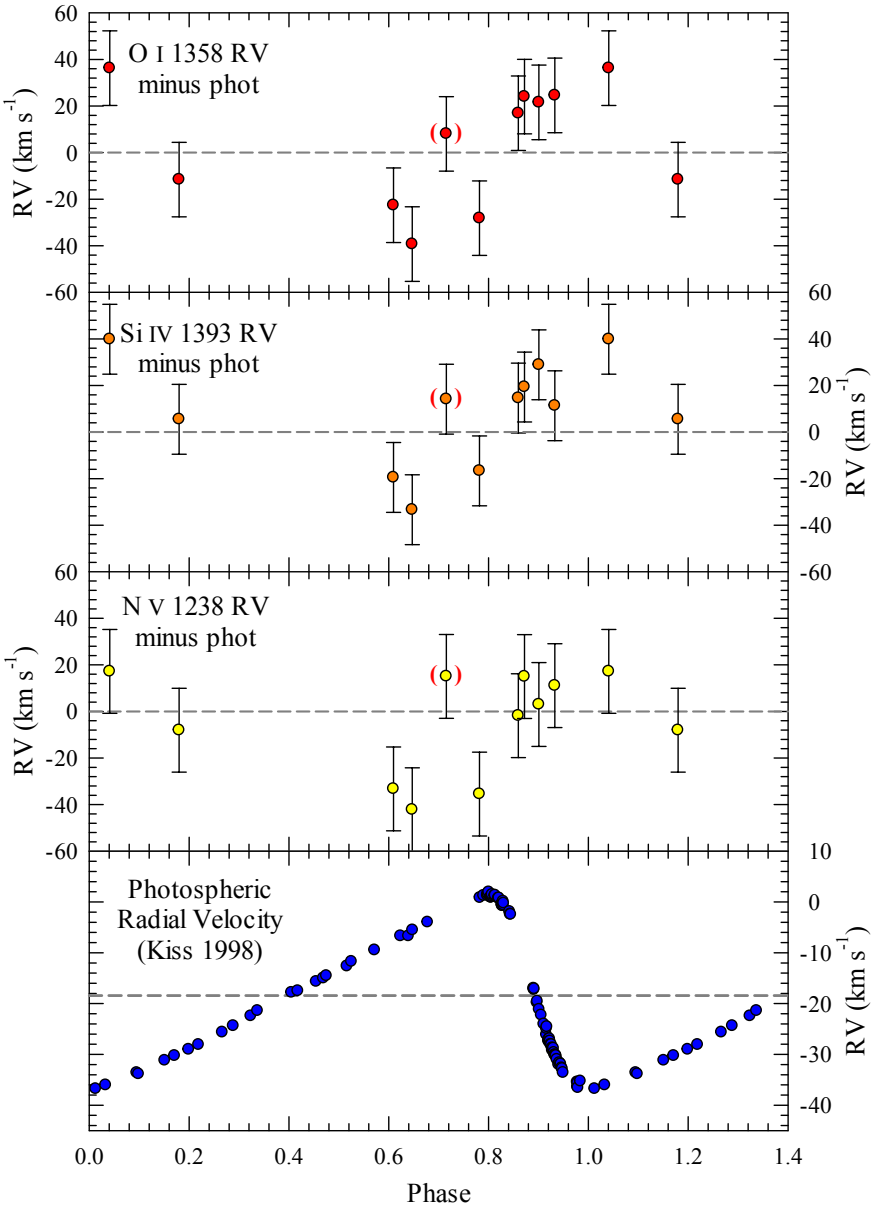

Fig. 7.— RVs determined for the *COS*-observed emission lines of δ Cep are shown vs. phase. The emission line velocities have the photospheric velocities (bottom panel) removed. The bracketed RV point is from a spectrum with a possible wavelength discrepancy, but the lack of continuum flux prevents us from confirming via photospheric or ISM absorption lines. For comparison, we have again included the photospheric RVs from Kiss (1998) in the bottom panel.

A. Photometry

The *UBVRI* photoelectric data for δ Cep, carried out with the *FCAPT* for this study, are given in Table 4. The data were obtained between December 2007 and January 2012.

Table 4. FCAPT *UBVRI* Photometry of δ CepTable 4

HJD	Phase	V-mag	error	HJD	Phase	U-B	error	HJD	Phase	B-V	error	HJD	Phase	V-R	error	HJD	Phase	R-I	error
2454437.5956	-0.2357	4.3136	0.0026	2454437.5926	-0.2362	0.6518	0.0060	2454437.5941	-0.2360	0.8588	0.0062	2454623.9116	0.4846	0.8475	0.0133	2454623.9118	0.4846	0.4449	0.0182
2454439.5928	0.1365	3.6690	0.0056	2454439.5941	0.1367	0.3887	0.0216	2454439.5928	0.1365	0.5839	0.0104	2454624.9074	-0.3299	0.8906	0.0133	2454624.9076	-0.3298	0.4568	0.0213
2454440.5858	0.3215	3.9369	0.0015	2454440.5856	0.3215	0.5173	0.0081	2454440.5857	0.3215	0.7411	0.0058	2454625.9097	-0.1431	0.8115	0.0306	2454625.9099	-0.1431	0.3999	0.0298
2454447.5794	-0.3752	4.2614	0.0029	2454447.5806	-0.3750	0.6512	0.0043	2454447.5793	-0.3752	0.8752	0.0035	2454626.9008	0.0416	0.6316	0.1148	2454626.9010	0.0416	0.3114	0.1183
2454449.5797	-0.0024	3.4627	0.0206	2454449.5795	-0.0025	0.3408	0.0429	2454449.5797	-0.0024	0.4522	0.0270	2454628.8955	0.4133	0.8242	0.0368	2454628.8957	0.4134	0.4223	0.0388
2454450.5797	0.1839	3.7435	0.0051	2454450.5795	0.1839	0.4299	0.0150	2454450.5797	0.1839	0.6358	0.0064	2454630.8917	-0.2147	0.8686	0.0130	2454630.8919	-0.2147	0.4471	0.0157
2454452.6001	-0.4396	4.1927	0.0008	2454452.6000	-0.4396	0.6393	0.0033	2454452.6001	-0.4396	0.8575	0.0028	2454631.8928	-0.0281	0.6187	0.0376	2454631.8930	-0.0281	0.3017	0.0322
2454454.5902	-0.0687	3.6357	0.0080	2454454.5914	-0.0685	0.3344	0.0223	2454454.5901	-0.0687	0.5130	0.0192	2454634.8827	-0.4710	0.8436	0.0104	2454634.8829	-0.4709	0.4573	0.0132
2454458.6295	-0.3160	4.3210	0.0038	2454458.6293	-0.3160	0.6698	0.0066	2454458.6294	-0.3160	0.8739	0.0075	2454636.8755	-0.0996	0.7132	0.0159	2454636.8757	-0.0996	0.3449	0.0187
2454459.6007	-0.1350	4.0087	0.0061	2454459.6005	-0.1350	0.4212	0.0188	2454459.6007	-0.1350	0.6829	0.0087	2454637.9467	0.1000	0.6852	0.0240	2454637.9469	0.1001	0.3425	0.0154
2454460.6012	0.0514	3.5319	0.0044	2454460.6010	0.0514	0.3427	0.0241	2454460.6011	0.0514	0.4928	0.0098	2454638.8722	0.2725	0.7897	0.0339	2454638.8724	0.2725	0.4029	0.0381
2454465.5856	-0.0197	3.4726	0.0097	2454465.5854	-0.0197	0.3114	0.0393	2454465.5855	-0.0197	0.4432	0.0161	2454640.8665	-0.3559	0.8592	0.0332	2454640.8667	-0.3558	0.4639	0.0394
2454466.5860	0.1667	3.7179	0.0030	2454466.5858	0.1667	0.4135	0.0243	2454466.5860	0.1667	0.6152	0.0090	2455098.6397	-0.0492	0.6392	0.0147	2455098.6399	-0.0492	0.3083	0.0179
2454623.9115	0.4845	4.0934	0.0069	2454623.9125	0.4847	0.5818	0.0075	2454623.9114	0.4845	0.8290	0.0102	2455098.8062	-0.0182	0.6168	0.0112	2455098.8064	-0.0182	0.2922	0.0067
2454624.9073	-0.3299	4.2869	0.0101	2454624.9096	-0.3295	0.6965	0.0045	2454624.9072	-0.3299	0.8948	0.0110	2455099.6797	0.1446	0.7060	0.0267	2455099.6799	0.1446	0.3626	0.0325
2454625.9096	-0.1431	4.0377	0.0132	2454625.9119	-0.1427	0.4678	0.0181	2454625.9095	-0.1431	0.6995	0.0203	2455099.8099	0.1688	0.7150	0.0091	2455099.8101	0.1689	0.3659	0.0079
2454626.9007	0.0416	3.5028	0.0736	2454626.9005	0.0415	0.3168	0.1136	2454626.9006	0.0416	0.4855	0.1044	2455100.6798	0.3309	0.7976	0.0147	2455100.6800	0.3310	0.4048	0.0113
2454628.8954	0.4133	4.0524	0.0255	2454628.8952	0.4133	0.5968	0.0100	2454628.8953	0.4133	0.7961	0.0272	2455100.8050	0.3543	0.7972	0.0098	2455100.8052	0.3543	0.4187	0.0084
2454630.8915	-0.2147	4.2666	0.0064	2454630.8914	-0.2147	0.6220	0.0067	2454630.8915	-0.2147	0.8435	0.0091	2455101.8010	-0.4601	0.8341	0.0063	2455101.8012	-0.4601	0.4423	0.0075
2454631.8927	-0.0282	3.4735	0.0338	2454631.8925	-0.0282	0.3129	0.0547	2454631.8926	-0.0282	0.4578	0.0472	2455102.6711	-0.2980	0.8716	0.0120	2455102.6713	-0.2979	0.4458	0.0148
2454634.8826	-0.4710	4.1342	0.0059	2454634.8837	-0.4708	0.6428	0.0085	2454634.8825	-0.4710	0.8499	0.0103	2455102.7988	-0.2742	0.8655	0.0043	2455102.7989	-0.2742	0.4518	0.0037
2454636.8754	-0.0996	3.8125	0.0075	2454636.8752	-0.0997	0.3607	0.0195	2454636.8753	-0.0996	0.5974	0.0164	2455106.7865	0.4689	0.8297	0.0105	2455106.7867	0.4690	0.4382	0.0095
2454637.9466	0.1000	3.5949	0.0221	2454637.9464	0.1000	0.3873	0.0198	2454637.9465	0.1000	0.5456	0.0281	2455131.7560	0.1220	0.6839	0.0093	2455131.7562	0.1221	0.3430	0.0087
2454638.8721	0.2725	3.8548	0.0283	2454638.8719	0.2724	0.4832	0.0229	2454638.8720	0.2724	0.6989	0.0339	2455133.7728	0.4979	0.8295	0.0112	2455133.7730	0.4979	0.4465	0.0096
2454640.8664	-0.3559	4.2744	0.0198	2454640.8712	-0.3550	0.6568	0.0127	2454640.8688	-0.3554	0.8617	0.0228	2455134.7811	-0.3142	0.8777	0.0105	2455134.7813	-0.3142	0.4600	0.0121
2455098.6395	-0.0493	3.5439	0.0031	2455098.6394	-0.0493	0.3202	0.0300	2455098.6395	-0.0493	0.4703	0.0115	2455135.7812	-0.1279	0.7493	0.0051	2455135.7814	-0.1278	0.3802	0.0063
2455098.8061	-0.0182	3.4698	0.0098	2455098.8059	-0.0183	0.3162	0.0282	2455098.8060	-0.0182	0.4468	0.0147	2455136.7803	0.0583	0.6346	0.0162	2455136.7805	0.0584	0.3161	0.0164
2455099.6796	0.1445	3.6712	0.0174	2455099.6794	0.1445	0.3933	0.0283	2455099.6795	0.1445	0.5873	0.0251	2455143.7568	0.3584	0.7916	0.0094	2455143.7570	0.3584	0.4198	0.0095
2455099.8098	0.1688	3.7231	0.0083	2455099.8096	0.1688	0.3957	0.0177	2455099.8097	0.1688	0.6079	0.0111	2455144.7440	-0.4576	0.8426	0.0040	2455144.7442	-0.4576	0.4436	0.0044
2455100.6797	0.3309	3.9503	0.0098	2455100.6795	0.3309	0.4961	0.0188	2455100.6796	0.3309	0.7481	0.0099	2455145.7525	-0.2697	0.8528	0.0057	2455145.7527	-0.2697	0.4529	0.0047
2455100.8049	0.3542	3.9894	0.0057	2455100.8047	0.3542	0.5408	0.0110	2455100.8049	0.3543	0.7592	0.0064	2455146.7368	-0.0863	0.6751	0.0133	2455146.7370	-0.0862	0.3376	0.0091
2455101.8009	-0.4601	4.1662	0.0051	2455101.8007	-0.4602	0.6152	0.0068	2455101.8008	-0.4602	0.8436	0.0056	2455151.7215	-0.1574	0.7938	0.0089	2455151.7217	-0.1573	0.4094	0.0075
2455102.6697	-0.2982	4.3076	0.0037	2455102.6695	-0.2983	0.6399	0.0111	2455102.6696	-0.2983	0.8748	0.0098	2455468.8626	-0.0577	0.6324	0.0083	2455468.8628	-0.0577	0.3048	0.0098
2455102.7986	-0.2742	4.3196	0.0036	2455102.7984	-0.2743	0.6272	0.0052	2455102.7986	-0.2742	0.8799	0.0044	2455469.8525	0.1268	0.6848	0.0109	2455469.8527	0.1268	0.3427	0.0078
2455106.7864	0.4689	4.0959	0.0071	2455106.7862	0.4689	0.5972	0.0116	2455106.7863	0.4689	0.8225	0.0090	2455470.8497	0.3126	0.7778	0.0119	2455470.8499	0.3126	0.4063	0.0100
2455131.7559	0.1220	3.6400	0.0047	2455131.7557	0.1220	0.3726	0.0261	2455131.7558	0.1220	0.5682	0.0131	2455471.8479	0.4986	0.8250	0.0085	2455471.8481	0.4987	0.4364	0.0092
2455133.7727	0.4978	4.1171	0.0079	2455133.7725	0.4978	0.6057	0.0094	2455133.7726	0.4978	0.8312	0.0087	2455476.8329	0.4276	0.8102	0.0108	2455476.8331	0.4276	0.4323	0.0127
2455134.7810	-0.3143	4.3066	0.0058	2455134.7808	-0.3143	0.6630	0.0104	2455134.7810	-0.3143	0.8879	0.0103	2455477.8318	-0.3863	0.8584	0.0070	2455477.8320	-0.3862	0.4547	0.0083
2455135.7811	-0.1279	3.9710	0.0016	2455135.7809	-0.1279	0.4214	0.0131	2455135.7810	-0.1279	0.6597	0.0042	2455478.8279	-0.2007	0.8286	0.0038	2455478.8281	-0.2006	0.4406	0.0048
2455136.7802	0.0583	3.5396	0.0107	2455136.7800	0.0583	0.3263	0.0237	2455136.7801	0.0583	0.5041	0.0139	2455479.8261	-0.0146	0.6120	0.0090	2455479.8263	-0.0146	0.2867	0.0101
2455143.7567	0.3584	3.9866	0.0033	2455143.7565	0.3583	0.5265	0.0077	2455143.7566	0.3584	0.7666	0.0068	2455480.8225	0.1710	0.7142	0.0151	2455480.8227	0.1711	0.3588	0.0147
2455144.7438	-0.4577	4.1803	0.0026	2455144.7449	-0.4575	0.6064	0.0024	2455144.7438	-0.4577	0.8490	0.0032	2455481.8207	0.3571	0.7908	0.0090	2455481.8209	0.3571	0.4168	0.0099
2455145.7524	-0.2697	4.3230	0.0037	2455145.7535	-0.2695	0.6619	0.0052	2455145.7523	-0.2697	0.8749	0.0049	2455482.8168	-0.4573	0.8476	0.0022	2455482.8170	-0.4573	0.4427	0.0055
2455146.7367	-0.0863	3.7385	0.0118	2455146.7378	-0.0861	0.3430	0.0261	2455146.7366	-0.0863	0.5586	0.0177	2455488.8023	-0.3419	0.8648	0.0057	2455488.8025	-0.3419	0.4536	0.0050
2455151.7214	-0.1574	4.1278	0.0068	2455151.7212	-0.1574	0.4719	0.0093	2455151.7214	-0.1574	0.7403	0.0095	2455492.8072	0.4044	0.8116	0.0069	2455492.8074	0.4044	0.4269	0.0051
2455468.8625	-0.0577	3.5880	0.0058	2455468.8623	-0.0578	0.2636	0.0332	2455468.8624	-0.0577	0.4836	0.0086	2455493.7962	-0.4113	0.8532	0.0073	2455493.7964	-0.4113	0.4506	0.0078
2455469.8524	0.1267	3.6395	0.0091	2455469.8522	0.1267	0.3709	0.0277	2455469.8523	0.1267	0.5750	0.0101	2455495.7965	-0.0385	0.6257	0.0089	2455495.7967	-0.0385	0.2863	0.0159
2455470.8496	0.3126	3.9216	0.0090	2455470.8506	0.3128	0.4550	0.0090	2455470.8495	0.3126	0.7337	0.0107	2455498.7914	-0.4804	0.8334	0.0042	2455498.7916	-0.4804	0.4434	0.0021
2455471.8477	0.4986	4.1325	0.0074	2455471.8476	0.4986	0.5523	0.0085	2455471.8477	0.4986	0.8203	0.0075	2455499.7862	-0.2950	0.8576	0.0082	2455499.7864	-0.2950	0.4483	0.0096
2455476.8328	0.4275	4.0543	0.0066	2455476.8326	0.4275	0.5565	0.0078	2455476.8328	0.4276	0.7966	0.0079	2455501.7760	0.0758	0.6490	0.0141	2455501.7761	0.0758	0.3168	0.0154
2455477.8317	-0.3863	4.2534	0.0037	2455477.8315	-0.3863	0.6369	0.0067	2455477.8317	-0.3863	0.8640	0.0050	2455502.7737	0.2617	0.7618	0.0091	2455502.7739	0.2617	0.3878	0.0057

Table 4—Continued

HJD	Phase	V-mag	error	HJD	Phase	U-B	error	HJD	Phase	B-V	error	HJD	Phase	V-R	error	HJD	Phase	R-I	error
2455478.8278	-0.2007	4.2579	0.0035	2455478.8288	-0.2005	0.5306	0.0030	2455478.8277	-0.2007	0.8274	0.0043	2455503.7705	0.4474	0.8195	0.0057	2455503.7707	0.4475	0.4345	0.0047
2455479.8259	-0.0147	3.4598	0.0058	2455479.8258	-0.0147	0.2990	0.0374	2455479.8259	-0.0147	0.4438	0.0124	2455504.7678	-0.3667	0.8593	0.0076	2455504.7679	-0.3667	0.4492	0.0054
2455480.8224	0.1710	3.7180	0.0116	2455480.8222	0.1710	0.3776	0.0215	2455480.8223	0.1710	0.6115	0.0154	2455506.7644	0.0054	0.6110	0.0125	2455506.7633	0.0051	0.2903	0.0178
2455481.8206	0.3570	3.9785	0.0029	2455481.8204	0.3570	0.5003	0.0195	2455481.8205	0.3570	0.7636	0.0049	2455508.7577	0.3768	0.8131	0.0051	2455508.7579	0.3768	0.4182	0.0051
2455482.8167	-0.4573	4.1735	0.0006	2455482.8165	-0.4574	0.6105	0.0096	2455482.8166	-0.4574	0.8388	0.0063	2455510.7524	-0.2515	0.8705	0.0049	2455510.7526	-0.2514	0.4505	0.0052
2455488.8022	-0.3419	4.2813	0.0050	2455488.8033	-0.3417	0.6661	0.0053	2455488.8034	-0.3417	0.8781	0.0051	2455511.7500	-0.0656	0.6559	0.0093	2455511.7502	-0.0655	0.3113	0.0094
2455492.8071	0.4044	4.0341	0.0058	2455492.8069	0.4044	0.5646	0.0185	2455492.8070	0.4044	0.7843	0.0097	2455512.7464	0.1201	0.6888	0.0080	2455512.7466	0.1201	0.3422	0.0100
2455493.7961	-0.4113	4.2234	0.0036	2455493.7959	-0.4113	0.6438	0.0093	2455493.7960	-0.4113	0.8642	0.0054	2455513.7467	0.3065	0.7853	0.0058	2455513.7469	0.3065	0.4056	0.0047
2455495.7963	-0.0386	3.5080	0.0040	2455495.7962	-0.0386	0.3188	0.0224	2455495.7963	-0.0386	0.4529	0.0059	2455515.7440	-0.3213	0.8583	0.0084	2455515.7442	-0.3213	0.4594	0.0066
2455498.7913	-0.4805	4.1397	0.0038	2455498.7911	-0.4805	0.5898	0.0089	2455498.7913	-0.4804	0.8403	0.0063	2455516.7383	-0.1360	0.7643	0.0068	2455516.7384	-0.1360	0.3856	0.0085
2455499.7861	-0.2951	4.3109	0.0060	2455499.7872	-0.2949	0.6147	0.0060	2455499.7860	-0.2951	0.8810	0.0075	2455532.6063	-0.1790	0.8205	0.0040	2455532.6065	-0.1789	0.4245	0.0019
2455501.7758	0.0757	3.5584	0.0083	2455502.7734	0.2616	0.4184	0.0107	2455501.7758	0.0757	0.5080	0.0131	2455532.6854	-0.1642	0.8072	0.0039	2455532.6856	-0.1642	0.4113	0.0024
2455502.7736	0.2617	3.8492	0.0084	2455503.7702	0.4474	0.5650	0.0081	2455502.7735	0.2616	0.6962	0.0085	2455533.5941	0.0051	0.6192	0.0055	2455533.5943	0.0051	0.2939	0.0052
2455503.7704	0.4474	4.0703	0.0041	2455504.7687	-0.3666	0.6450	0.0064	2455503.7703	0.4474	0.8109	0.0073	2455862.6718	0.3292	0.7970	0.0059	2455862.6720	0.3292	0.4151	0.0039
2455504.7676	-0.3668	4.2629	0.0068	2455506.7628	0.0051	0.3137	0.0261	2455504.7676	-0.3668	0.8764	0.0087	2455865.6113	-0.1231	0.7487	0.0054	2455865.6114	-0.1230	0.3780	0.0073
2455506.7656	0.0056	3.4644	0.0101	2455508.7574	0.3767	0.4885	0.0094	2455506.7642	0.0053	0.4493	0.0161	2455866.5963	0.0605	0.6474	0.0064	2455866.5964	0.0605	0.3171	0.0048
2455508.7576	0.3768	4.0027	0.0015	2455510.7521	-0.2515	0.6259	0.0038	2455508.7575	0.3768	0.7787	0.0063	2455867.5955	0.2467	0.7607	0.0056	2455867.5957	0.2467	0.3860	0.0058
2455510.7523	-0.2515	4.3192	0.0031	2455511.7497	-0.0656	0.3313	0.0237	2455510.7522	-0.2515	0.8726	0.0042	2455868.5951	0.4330	0.8311	0.0035	2455868.5952	0.4330	0.4313	0.0053
2455511.7498	-0.0656	3.6148	0.0078	2455512.7461	0.1200	0.3340	0.0193	2455511.7498	-0.0656	0.5041	0.0247	2455881.5652	-0.1500	0.7904	0.0045	2455881.5653	-0.1500	0.4069	0.0046
2455512.7463	0.1201	3.6349	0.0040	2455513.7464	0.3065	0.4628	0.0073	2455512.7462	0.1201	0.5566	0.0100	2455881.5800	-0.1473	0.7815	0.0030	2455881.5802	-0.1472	0.4031	0.0031
2455513.7465	0.3065	3.9130	0.0042	2455515.7437	-0.3213	0.6444	0.0078	2455513.7465	0.3065	0.7305	0.0070	2455881.5949	-0.1445	0.7834	0.0067	2455881.5950	-0.1445	0.3968	0.0064
2455515.7439	-0.3213	4.2962	0.0067	2455516.7379	-0.1361	0.3991	0.0162	2455515.7438	-0.3213	0.8734	0.0084	2455881.6098	-0.1417	0.7768	0.0053	2455881.6099	-0.1417	0.3948	0.0038
2455516.7381	-0.1360	4.0154	0.0058	2455532.6060	-0.1790	0.5079	0.0084	2455516.7381	-0.1360	0.6895	0.0087	2455881.6246	-0.1390	0.7713	0.0041	2455881.6248	-0.1389	0.3922	0.0049
2455532.6062	-0.1790	4.1985	0.0037	2455532.6851	-0.1643	0.4582	0.0140	2455532.6061	-0.1790	0.7854	0.0039	2455881.6396	-0.1362	0.7630	0.0063	2455881.6397	-0.1361	0.3914	0.0066
2455532.6853	-0.1643	4.1480	0.0034	2455533.5938	0.0050	0.3076	0.0636	2455532.6852	-0.1643	0.7549	0.0081	2455881.6542	-0.1334	0.7657	0.0067	2455881.6543	-0.1334	0.3871	0.0052
2455533.5940	0.0051	3.4631	0.0044	2455862.6716	0.3291	0.5273	0.0073	2455533.5939	0.0051	0.4426	0.0056	2455881.6688	-0.1307	0.7597	0.0032	2455881.6689	-0.1307	0.3864	0.0047
2455862.6718	0.3292	3.9454	0.0048	2455865.6121	-0.1229	0.4116	0.0161	2455862.6717	0.3291	0.7361	0.0058	2455881.6834	-0.1280	0.7515	0.0079	2455881.6835	-0.1280	0.3776	0.0049
2455865.6113	-0.1231	3.9479	0.0047	2455866.5960	0.0604	0.3642	0.0151	2455865.6112	-0.1231	0.6473	0.0085	2455881.6981	-0.1253	0.7551	0.0035	2455881.6982	-0.1252	0.3733	0.0042
2455866.5962	0.0605	3.5297	0.0046	2455867.5953	0.2467	0.4690	0.0202	2455866.5962	0.0605	0.4819	0.0056	2455881.7128	-0.1225	0.7531	0.0084	2455881.7129	-0.1225	0.3776	0.0074
2455867.5955	0.2467	3.8237	0.0048	2455868.5949	0.4329	0.5862	0.0089	2455867.5954	0.2467	0.6749	0.0078	2455881.7274	-0.1198	0.7378	0.0052	2455881.7276	-0.1198	0.3727	0.0050
2455868.5950	0.4330	4.0575	0.0014	2455881.5649	-0.1501	0.4587	0.0050	2455868.5950	0.4330	0.8013	0.0030	2455882.7387	0.0687	0.6529	0.0120	2455882.7389	0.0687	0.3096	0.0122
2455881.5651	-0.1500	4.0841	0.0023	2455881.5798	-0.1473	0.4551	0.0141	2455881.5651	-0.1500	0.7125	0.0035	2455888.7209	0.1835	0.7202	0.0049	2455888.7210	0.1835	0.3609	0.0049
2455881.5800	-0.1473	4.0662	0.0026	2455881.5946	-0.1445	0.4413	0.0064	2455881.5799	-0.1473	0.7114	0.0043	2455892.6969	-0.0756	0.6567	0.0080	2455892.6971	-0.0756	0.3329	0.0099
2455881.5948	-0.1445	4.0545	0.0033	2455881.6095	-0.1418	0.4362	0.0135	2455881.5947	-0.1445	0.7006	0.0052	2455893.7074	0.1127	0.6821	0.0075	2455893.7075	0.1127	0.3441	0.0047
2455881.6097	-0.1417	4.0402	0.0042	2455881.6244	-0.1390	0.4287	0.0077	2455881.6096	-0.1417	0.6987	0.0069	2455900.6875	0.4134	0.8189	0.0075	2455900.6877	0.4135	0.4316	0.0063
2455881.6246	-0.1390	4.0255	0.0036	2455881.6393	-0.1362	0.4173	0.0093	2455881.6245	-0.1390	0.6893	0.0044	2455911.6610	0.4584	0.8345	0.0057	2455911.6611	0.4584	0.4278	0.0082
2455881.6395	-0.1362	4.0084	0.0047	2455881.6539	-0.1335	0.4129	0.0020	2455881.6394	-0.1362	0.6861	0.0073	2455912.6203	-0.3629	0.8583	0.0074	2455912.6204	-0.3628	0.4601	0.0050
2455881.6541	-0.1335	3.9959	0.0056	2455881.6685	-0.1308	0.4136	0.0092	2455881.6541	-0.1335	0.6806	0.0058	2455919.5649	-0.0687	0.6601	0.0076	2455919.5650	-0.0687	0.3246	0.0104
2455881.6687	-0.1307	3.9808	0.0021	2455881.6832	-0.1280	0.4107	0.0057	2455881.6687	-0.1307	0.6726	0.0056	2455919.5806	-0.0658	0.6615	0.0101	2455919.5796	-0.0660	0.3160	0.0112
2455881.6833	-0.1280	3.9622	0.0076	2455881.6978	-0.1253	0.4064	0.0085	2455881.6833	-0.1280	0.6657	0.0087	2455919.5947	-0.0632	0.6539	0.0117	2455919.5948	-0.0632	0.3128	0.0101
2455881.6980	-0.1253	3.9496	0.0025	2455881.7125	-0.1226	0.3926	0.0164	2455881.6980	-0.1253	0.6482	0.0061	2455919.6069	-0.0609	0.6510	0.0114	2455919.6070	-0.0609	0.3162	0.0140
2455881.7127	-0.1225	3.9351	0.0048	2455881.7272	-0.1198	0.3862	0.0083	2455881.7127	-0.1225	0.6463	0.0061	2455919.6215	-0.0582	0.6572	0.0092	2455919.6217	-0.0581	0.2988	0.0087
2455881.7274	-0.1198	3.9171	0.0030	2455882.7385	0.0686	0.3482	0.0101	2455881.7273	-0.1198	0.6407	0.0066	2455922.6360	-0.4964	0.8478	0.0065	2455922.6361	-0.4964	0.4338	0.0039
2455882.7387	0.0687	3.5467	0.0059	2455888.7206	0.1834	0.4150	0.0201	2455882.7386	0.0686	0.5016	0.0065	2455926.6212	0.2462	0.7505	0.0086	2455926.6214	0.2463	0.3917	0.0088
2455888.7209	0.1834	3.7327	0.0025	2455892.6967	-0.0757	0.3329	0.0126	2455888.7208	0.1834	0.6285	0.0045	2455927.6224	0.4328	0.8066	0.0098	2455927.6225	0.4328	0.4227	0.0108
2455892.6969	-0.0756	3.6782	0.0051	2455893.7072	0.1127	0.3696	0.0104	2455892.6968	-0.0756	0.5418	0.0128	2455931.6091	0.1757	0.7170	0.0067	2455931.6092	0.1757	0.3588	0.0071
2455893.7074	0.1127	3.6233	0.0062	2455900.6873	0.4134	0.5663	0.0066	2455893.7073	0.1127	0.5509	0.0072								
2455900.6875	0.4134	4.0396	0.0048	2455911.6608	0.4583	0.5911	0.0063	2455900.6874	0.4134	0.7927	0.0068								
2455911.6610	0.4584	4.0806	0.0023	2455912.6201	-0.3629	0.6577	0.0056	2455911.6609	0.4584	0.8116	0.0054								
2455912.6203	-0.3629	4.2621	0.0061	2455919.5647	-0.0688	0.3442	0.0165	2455912.6202	-0.3629	0.8832	0.0077								
2455919.5649	-0.0687	3.6346	0.0062	2455919.5793	-0.0660	0.3317	0.0183	2455919.5648	-0.0687	0.5022	0.0125								

Table 4—Continued

HJD	Phase	V-mag	error	HJD	Phase	U-B	error	HJD	Phase	B-V	error	HJD	Phase	V-R	error	HJD	Phase	R-I	error
2455919.5816	-0.0656	3.6206	0.0063	2455919.5944	-0.0632	0.3344	0.0118	2455919.5805	-0.0658	0.5072	0.0098								
2455919.5946	-0.0632	3.6030	0.0111	2455919.6066	-0.0610	0.3326	0.0126	2455919.5946	-0.0632	0.4904	0.0152								
2455919.6068	-0.0609	3.5938	0.0103	2455919.6213	-0.0582	0.3053	0.0177	2455919.6067	-0.0609	0.4928	0.0126								
2455919.6215	-0.0582	3.5778	0.0056	2455922.6358	-0.4965	0.5951	0.0057	2455919.6214	-0.0582	0.4911	0.0056								
2455922.6360	-0.4964	4.1270	0.0054	2455926.6210	0.2462	0.4516	0.0113	2455922.6359	-0.4964	0.8262	0.0065								
2455926.6211	0.2462	3.8209	0.0048	2455927.6222	0.4328	0.5737	0.0143	2455926.6211	0.2462	0.6892	0.0083								
2455927.6223	0.4328	4.0375	0.0060	2455931.6089	0.1757	0.3997	0.0097	2455927.6223	0.4328	0.8152	0.0090								
2455931.6091	0.1757	3.7166	0.0021					2455931.6090	0.1757	0.6286	0.0046								

REFERENCES

Adelman, S. J., Boyd, L., Dukes, R. J., Jr., et al. 2001, IAU General Assembly, 24, 314

Aloisi, A., Ake, T., Bostroem, A., et al. 2010, Hubble after SM4. Preparing JWST,

Anderson, R. I., Ekström, S., Georgy, C., et al. 2014, A&A, 564, A100

Andrievsky, S. M., Luck, R. E., & Kovtyukh, V. V. 2005, AJ, 130, 1880

Ayres, T. R. 2011, ApJ, 738, 120

Ayres, T. R., Brown, A., & Harper, G. M. 2005, ApJ, 627, L53

Bahner, K., Hiltner, W. A., & Kraft, R. P. 1962, ApJS, 6, 319

Barnes, T. G., III, Fernley, J. A., Frueh, M. L., et al. 1997, PASP, 109, 645

Basri, G., Clarke, J. T., & Haisch, B. M. 1985, A&A, 144, 161

Benedict, G. F., McArthur, B. E., Feast, M. W., et al. 2007, AJ, 133, 1810

Berdnikov, L. N., Ignatova, V. V., Caldwell, J. A. R., & Koen, C. 2000, New A, 4, 625

Bohm-Vitense, E., & Love, S. G. 1994, ApJ, 420, 401

Caputo, F., Bono, G., Fiorentino, G., Marconi, M., & Musella, I. 2005, ApJ, 629, 1021

Cassisi, S., & Salaris, M. 2011, ApJ, 728, L43

Davis, J. J., Tracey, J. C., Engle, S. G., & Guinan, E. F. 2002, Bulletin of the American Astronomical Society, 34, #117.11

de Zeeuw, P. T., Hoogerwerf, R., de Bruijne, J. H. J., Brown, A. G. A., & Blaauw, A. 1999, AJ, 117, 354

Drake, S. A., Singh, K. P., White, N. E., Mewe, R., & Kaastra, J. S. 1996, Cool Stars, Stellar Systems, and the Sun, 109, 263

Doyle, J. G., O'Shea, E., Erdelyi, R., et al. 1997, Sol. Phys., 173, 243

Engle, S. G., & Guinan, E. F. 2012, Journal of Astronomy and Space Sciences, 29, 181

Engle, S. G., Guinan, E. F., & Koch, R. H. 2004, Bulletin of the American Astronomical Society, 36, 744

Evans, N. R., Guinan, E., Engle, S., et al. 2010, AJ, 139, 1968

Evans, N. R., Schaefer, G., Bond, H. E., et al. 2007, IAU Symposium, 240, 102

Fokin, A. B., Gillet, D., & Breitfellner, M. G. 1996, A&A, 307, 503

Goodricke, J., & Bayer, J. 1786, Royal Society of London Philosophical Transactions Series I, 76, 48

Guinan, E. F., & Engle, S. G. 2009, IAU Symposium, 258, 395

Kiss, L. L. 1998, MNRAS, 297, 825

Koncewicz, R., & Jordan, C. 2007, MNRAS, 374, 220

Linsky, J. L., Wood, B. E., Judge, P., et al. 1995, ApJ, 442, 381

Majaess, D., Turner, D., & Gieren, W. 2012, ApJ, 747, 145

Marengo, M., Evans, N. R., Matthews, L. D., et al. 2013, Stellar Pulsations: Impact of New Instrumentation and New Insights, 31, 99

Matthews, L. D., Marengo, M., Evans, N. R., & Bono, G. 2012, ApJ, 744, 53

Neilson, H. R., Langer, N., Engle, S. G., Guinan, E., & Izzard, R. 2012, ApJ, 760, L18

Neilson, H. R., Cantiello, M., & Langer, N. 2011, A&A, 529, L9

Pagano, I., Linsky, J. L., Carkner, L., et al. 2000, ApJ, 532, 497

Prugniel, P., Soubiran, C., Koleva, M., & Le Borgne, D. 2007, VizieR Online Data Catalog, 3251, 0

Sasselov, D. D., & Lester, J. B. 1994, ApJ, 423, 795

Schmidt, E. G., & Parsons, S. B. 1984, ApJ, 279, 202

Schmidt, E. G., & Parsons, S. B. 1984, ApJ, 279, 215

Schmidt, E. G., & Parsons, S. B. 1982, ApJS, 48, 185

Spreckley, S. A., & Stevens, I. R. 2008, MNRAS, 388, 1239

Turner, D. G., & Berdnikov, L. N. 2004, A&A, 423, 335

Turner, D. G., Bryukhanov, I. S., Balyuk, I. I., et al. 2007, PASP, 119, 1247

van Leeuwen, F., Feast, M. W., Whitelock, P. A., & Laney, C. D. 2007, MNRAS, 379, 723

Dufton, P. L., Hibbert, A., Kingston, A. E., & Doschek, G. A. 1983, ApJ, 274, 420

Dupree, A. K., Foukal, P. V., & Jordan, C. 1976, ApJ, 209, 621

Engle, S. G., Guinan, E. F., Depasquale, J., & Evans, N. 2009, American Institute of Physics Conference Series, 1135, 192

Evans, N. R. 1976, ApJS, 32, 399

Feldmeier, A., Kudritzki, R.-P., Palsa, R., Pauldrach, A. W. A., & Puls, J. 1997, A&A, 320, 899

Freedman, W. L., & Madore, B. F. 2010, ARA&A, 48, 673

Gillet, D., & Fokin, A. B. 2014, A&A, 565, A73

Gillet, D., Fokin, A. B., Breitfellner, M. G., Mazauric, S., & Nicolas, A. 1999, A&A, 344, 935

Hertzsprung, E. 1919, Astronomische Nachrichten, 210, 17

Keenan, F. P., Dufton, P. L., Kingston, A. E., & Cook, J. W. 1989, ApJ, 340, 1135

Komatsu, E., Smith, K. M., Dunkley, J., et al. 2011, ApJS, 192, 18

Marengo, M., Evans, N. R., Barmby, P., et al. 2010, ApJ, 725, 2392

Meyermann, B. 1904, Astronomische Nachrichten, 167, 1

Moffett, T. J., & Barnes, T. G., III 1980, ApJS, 44, 427

Morel, P., Provost, J., Pichon, B., Lebreton, Y., & Thévenin, F. 2010, A&A, 520, A41

Neilson, H. R., Engle, S. G., Guinan, E., et al. 2012, ApJ, 745, L32

Neilson, H. R., Langer, N., Engle, S. G., Guinan, E., & Izzard, R. 2012, ApJ, 760, L18

Neilson, H. R., & Lester, J. B. 2008, ApJ, 684, 569

Oskinova, L. M., Nazé, Y., Todt, H., et al. 2014, Nature Communications, 5,

Paresce, F. 1984, AJ, 89, 1022

Planck Collaboration, Ade, P. A. R., Aghanim, N., et al. 2013, arXiv:1303.5062

Riess, A. G., Macri, L., Casertano, S., et al. 2011, ApJ, 730, 119

Stebbins, J. 1908, ApJ, 27, 188

Szabados, L. 1980, Commmunications of the Konkoly Observatory Hungary, 76, 1

Willson, L. A., & Bowen, G. H. 1986, Irish Astronomical Journal, 17, 249

This preprint was prepared with the AAS LaTeX macros v5.2.